

# HIGH-PRESSURE EXPERIMENTS AND THE PHASE DIAGRAM OF LOWER MANTLE AND CORE MATERIALS

R. Boehler

*High-Pressure Mineral Physics  
Max-Planck Institut für Chemie  
Mainz, Germany*

**Abstract.** The interpretation of seismic data and computer modeling requires increased accuracy in relevant material properties in order to improve our knowledge of the structure and dynamics of the Earth's deep interior. To obtain such properties, a complementary method to classic shock compression experiments and theoretical calculations is the use of laser-heated diamond cells, which are now producing accurate data on phase diagrams, equations of state, and melting. Data on one of the most important measurements, the melting temperatures of iron at very high pressure, are now converging. Two other issues linking core properties to those of iron are investigated in the diamond cell: One is the melting point depression of iron in the presence of light elements, and the other is the structure of iron at the conditions of the inner core. First measurements on eutectic systems indicate a significant decrease in the melting point depression with increasing pressure, which is in contrast to previous predictions. X-ray diffraction measurements at simultaneously high pressure and high temperature have improved significantly with the instal-

lation of high-pressure "beam lines" at synchrotron facilities, and structural measurements on iron are in progress. Considerable efforts have been made to develop new techniques to heat minerals at the conditions of the deep mantle in the diamond cell and to measure their phase relations reliably. Even measurements of the melting behavior of realistic rock compositions at high pressure, previously considered to be impossible in the diamond cell, have been reported. The extrapolated solidus of the lower mantle intersects the geotherm at the core-mantle boundary, which may explain the seismically observed ultra low velocity zone. The diamond cell has great potential for future development and broad application, as new measurements on high-pressure geochemistry at deep mantle and core conditions have opened a new field of research. There are, however, strict experimental requirements for obtaining reliable data, which are summarized in the present paper. Results from recent measurements of melting temperatures and phase diagrams of lower mantle and core materials at very high pressure are reviewed.

## 1. INTRODUCTION

The interpretation of seismic data that have gained significantly in resolution and amount in the last few years poses a challenge in the fields of computer modeling, geochemistry, and experimental high-pressure research. A picture has evolved in which the Earth is much more heterogeneous in its internal structure than previously thought [Kellogg *et al.*, 1999], and the causes for these heterogeneities are only poorly understood. The observed lateral and depth variations in seismic velocities may have thermal, structural, dynamical, and/or chemical causes. A key element in the understanding of this complexity is the study of physical and chemical properties of the relevant Earth materials. However, at the very high pressure and temperature conditions of the Earth's deep interior the accurate measurement of physical and chemical material properties becomes exceedingly difficult. The two techniques capable of generating such high pressure and temperature conditions, shock-compression and laser heating in diamond cells, have

associated weaknesses. The primary drawback to shock compression experiments is the short timescale, and for the diamond cell the drawback is the small sample size. It is unfortunate but natural that the complexity in these techniques had initially led to very large discrepancies in geophysically important results, in particular the melting temperatures of iron, which are key for estimating the temperature in the Earth's center. Without the improvement of these techniques in the last few years, the uncertainty in these estimates would still far exceed 1000 K.

The purpose of this paper is to summarize the most important techniques to accurately characterize pressure, temperature, volume, and phase transitions in the laser-heated diamond cell, because seemingly minor experimental differences have been shown to cause very large discrepancies in the experimental results. These previous data have been recently comprehensively described [Shen and Heinz, 1998] and will not be reviewed here. Rather, an attempt is made to show where data have converged and where the results are still unresolved. Because discrepancies in data in most cases are

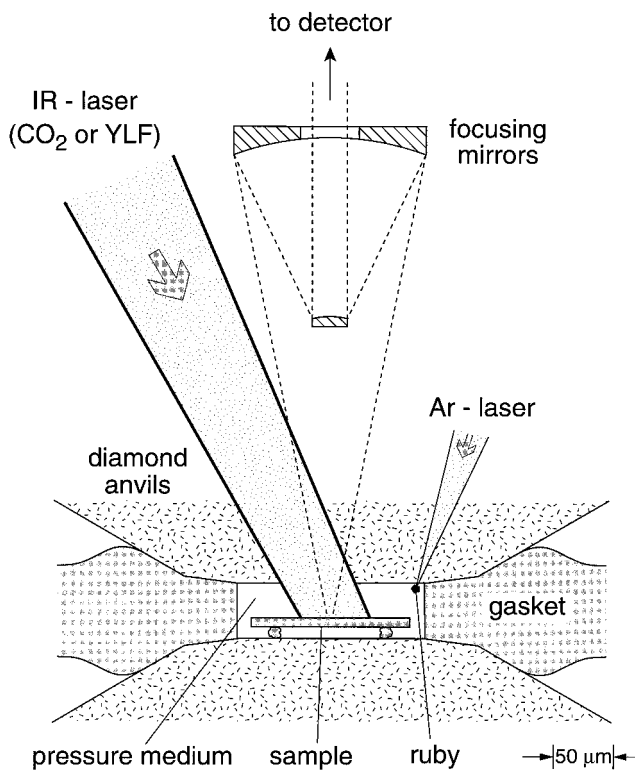


**Figure 1.** Schematic of a laser-heated diamond cell. Sample is thermally insulated from the diamonds by an inert, soft, low-conductivity pressure medium and absorbs most of the laser radiation. Laser absorption and emission of incandescent light by the pressure medium and the diamond anvil are negligible. Laser beam is defocused. Incandescent light is collected from a micron-sized area of the sample with mirror optics that are free of chromatic aberration. Pressure can be measured from unheated ruby chips during heating.

not simple data scatter, but a result of technical developments (or shortcomings), random averaging may not be wise. However, selecting data requires some knowledge of experimental details.

The experimental task is to simulate realistic conditions in the Earth's interior as closely as possible, namely, hydrostaticity, uniformity in temperature, and thermodynamic and chemical equilibrium. These requirements are difficult to achieve with any experimental high-pressure method, especially the ones capable of reaching pressures and temperatures of the Earth's lower mantle and core: shock wave experiments and laser-heated diamond cell experiments. (The pressure and temperature regime of multianvil devices is limited to that of the top of the lower mantle.) The shock wave technique allows accurate measurements of densities and sound velocities covering most of the  $P$ - $T$  range of the Earth, but because pressure and temperature are coupled, melting and phase changes for a given material can only be determined at one  $P$ - $T$  condition on the *Hugoniot*, and thus slopes of melting curves or phase boundaries cannot be determined. (Terms in italic are defined in the glossary, following the main text.)

Laser heating in diamond cells is capable of reaching pressure and temperature conditions of the Earth's core. The maximum pressure reported is 200 GPa [Boehler, 1993] at temperatures of 4000 K. Temperatures between 1200 and 6000 K can be easily achieved and measured accurately. The main advantage in using diamond cell over shock experiments is that  $P$ - $T$  conditions can be kept constant for long periods of time (hours), and this allows visual, spectroscopic, and X-ray diffraction measurements. Melting, which can be directly observed by a number of methods, can be measured over a large pressure range, yielding accurate melting slopes. Pressure correction upon heating is small, and the spectroscopic measurement of temperatures is straightforward, without the requirement of corrections once proper techniques are used (see below).

## 2. DIAMOND CELL AND BASIC EXPERIMENTAL TECHNIQUES

### 2.1. Properties of Diamonds

The principal components of a diamond cell are two diamond anvils compressing a gasket. A hole drilled in the center of the gasket serves as the pressure chamber. The strength, or the internal friction of the gasket (usually made of steel or hard metal), must be greater than the radial forces in the pressure chamber. At very high pressure this can only be achieved for gasket thicknesses of less than about 50  $\mu\text{m}$ , a great disadvantage in laser-heating experiments. Diamond possesses not only very high strength, but also very high thermal conductivity, about 5 times that of copper. The disadvantage of this property is that at high pressure a large portion of the heat produced in the sample by the laser is conducted away through the diamond anvils. Thus, in order to reach high temperatures in the sample, the laser beam in the earlier experiments had to be tightly focused because the laser power was limited. This, however, caused high temperature gradients. To circumvent this problem, the sample should be embedded in a pressure medium with low thermal conductivity that does not absorb the laser radiation. The laser beam can then be defocused, resulting in a much flatter temperature profile. A typical high-pressure cell arrangement for laser heating of this type is shown in Figure 1. For laser heating at laser wavelengths of 1  $\mu\text{m}$  (yttrium-aluminum-garnet (YAG) or yttrium-lithium-fluoride (YLF) lasers) or 10  $\mu\text{m}$  (the CO<sub>2</sub> laser) (see below), both type I or type IIA diamonds may be used. At 10  $\mu\text{m}$  wavelength, about 30–40% of the laser radiation is absorbed by a 2-mm-thick type I, and about 10% is absorbed by a type IIA diamond.

### 2.2. Pressure Medium

The requirements for the pressure medium for laser-heating experiments are (1) low shear strength, to minimize deviatoric stresses in the sample, (2) low thermal conductivity, in order to minimize laser focusing, (3)

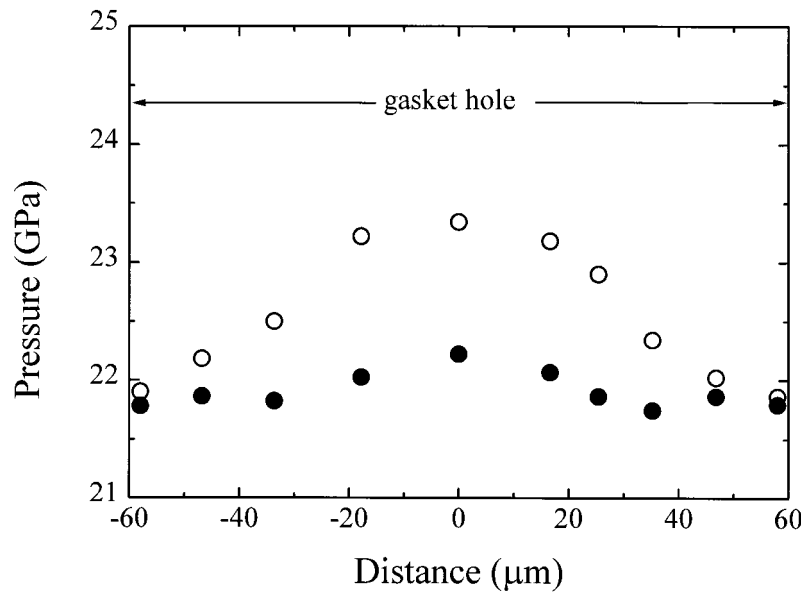


**Figure 2.** Pressure gradients in a diamond cell before (open circles) and after (solid circles) laser heating. For this measurement the ruby chips were distributed on the lower diamond in Figure 1. Stress gradients are almost fully relaxed after heating.

chemical inertness, (4) low absorption of the laser light, and (5) low emissivity, such that its emitted incandescent light is negligible in the measurement of the sample temperature. Ideal pressure media are the noble gases, which fulfill all requirements. Their disadvantage, however, is high compressibility, which at high pressures reduces the thickness of the thermally insulating layer between the sample and the diamond. Alkali halides, especially those exhibiting low thermal conductivity at high pressure (e.g., KBr, CsI, CsCl), are also well suited, but in some cases these react with the sample. Additionally, their high background fluorescence at high pressure often interferes with Raman (not with IR) spectroscopic measurements. It is often a time-consuming task to find the most suitable pressure medium for a given experimental problem because optical and thermal properties may change significantly at high pressure and high temperature. Very high pressures (above about 100 GPa) require sacrifices on ideal properties of the pressure medium, loss of hydrostaticity being the most important one. It is therefore important to check agreement between experimental data using hydrostatic and nonhydrostatic pressure media.

### 2.3. Pressure Measurements

Pressures in laser-heated diamond cells are measured routinely by the ruby fluorescence method [Mao *et al.*, 1978]. The accuracy of this pressure scale has been further tested recently by simultaneous Brillouin measurements on MgO [Zha *et al.*, 2000]. Ruby has a strong fluorescence spectrum with a large pressure shift but, unfortunately, also a large shift with temperature. Other materials have less of a temperature dependence, but the shift of their fluorescence spectra under simulta-

neous high pressure and high temperature is limited to the temperature at which the fluorescence decays (above about 800 K). Pressures in a laser-heated diamond cell with a hydrostatic pressure medium can be accurately measured, however, from unheated ruby chips anywhere in the pressure chamber. As pressure increases, so do the gradients, but when the sample is heated with the laser, the pressure medium heats by thermal conduction and then anneals, and the pressure gradients are significantly reduced, as is evident from Figure 2.

### 2.4. Thermal Pressure

To a first approximation the volume of the sample chamber in a diamond cell remains constant upon heating the sample with a laser. This causes an increase in pressure that is proportional to the temperature difference and depends on the thermal expansivity and the compressibility of the materials involved (sample and pressure medium). Because the temperature distribution in the sample chamber is very complicated, three-dimensional, and changes from run to run, calculations of the *thermal pressure* are uncertain. The problem can be circumvented by (1) choosing a hydrostatic pressure medium and measuring the pressure via the ruby scale in an unheated area in the medium (see Figure 1) or (2) measuring the density of the heated portion of the sample by X-ray diffraction using finely collimated *synchrotron radiation*.

The upper limit of the thermal pressure in the sample itself may be estimated: Stress gradients induced in laser-heated samples are limited by their yield strength, provided they are embedded in a soft pressure medium. A sample that is not uniformly heated will flow or crack if internal stress gradients exceed the elastic limit. At the

high temperatures of the laser-heated diamond cell the *yield strength* of most geological materials decreases to well below 1 GPa, thus limiting internal stress gradients to insignificant levels. In a molten sample embedded in a hydrostatic pressure medium, stress gradients are zero.

A separate issue is the pressure increase in the pressure chamber due to the thermal pressure in both the sample and the pressure medium. This pressure increase can be precisely measured when the cell geometry shown in Figure 1 is used. This thermal pressure increase is insignificant if the volume of the sample is small with respect to the volume of the pressure medium, as was the case in melting or phase transition measurements, where thermal pressures did not exceed 0.3 GPa [Boehler and Chopelas, 1991].

Conflicting results, however, have been reported recently [Fiquet et al., 1996] from X-ray measurements. Difficulties associated with X-ray diffraction will be described below. The main problems are the unknown  $P$ - $T$  equation of state of the sample, the large sample-to-pressure-medium ratio, and temperature gradients in the X-rayed portion of the sample.

## 2.5. Laser Heating

The principal requirements are high power, stability in power and beam position, suitable wavelength for absorption, and preferably a wavelength outside the spectral range in which the incandescent light from the sample is measured. Nd-doped yttrium-aluminum-garnet (YAG) ( $\lambda = 1.06 \mu\text{m}$ ) lasers, first used by Ming and Bassett [1974], and CO<sub>2</sub> lasers ( $\lambda = 10.6 \mu\text{m}$ ) [Boehler and Chopelas, 1991] have typical powers of 20 and 150 W, respectively. However, intrinsic power instability of these lasers produced temperature fluctuations of several hundred degrees, a serious problem for accurately measuring phase transitions. Nd-doped yttrium-lithium-fluoride lasers (YLF) ( $\lambda = 1.05 \mu\text{m}$ ) provide significantly higher stability of both power and beam position. CO<sub>2</sub> lasers can be stabilized with an electronic feedback mechanism, which uses the incandescent light of the sample to regulate the laser power [Boehler and Chopelas, 1991]. Both YLF and stabilized CO<sub>2</sub> lasers provide temperature stability within about 10 K.

## 2.6. Optics

In the early laser-heating experiments, microscopes served for both focusing the laser beam and observing the sample. This caused major problems: (1) The microscope objectives are designed for visible light, and the transmission of laser light at 1- $\mu\text{m}$  wavelength is significantly reduced due to reflection. Additionally, beam splitters (*dichroic mirrors*) have to be used to separate the laser radiation from the incandescent light coming from the heated sample, and this further reduces the laser power, resulting in a total loss in power of over 50%. (2) The sample is located in the focal point of the objective, and thus the laser beam is nearly focused, creating small hot spots with very large temperature

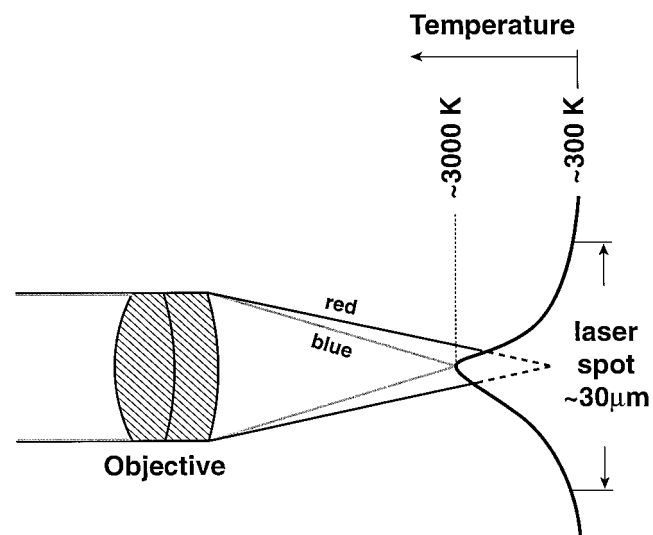


**Figure 3.** Problem associated with chromatic aberration of lens systems used for temperature measurement when large temperature gradients are present. For a standard microscope objective the focal distance between red and blue is about 30  $\mu\text{m}$ . The hot spot has a similar diameter. Therefore different temperatures are sampled at different wavelengths. This can cause systematic errors in the temperature measurements of the order of 1000 K, especially at high pressures when hot spots are small. For large hot spots with a flat temperature distribution (in low-pressure experiments or during optical calibration using tungsten ribbon lamps), chromatic aberration plays a minor role.

gradients. Moreover, microscopes are unsuitable for the use of CO<sub>2</sub> lasers because this radiation is fully absorbed by the glass lenses.

These problems are avoided by using separate lenses for focusing the laser beam with suitable antireflection coatings, providing a throughput of over 95% of the laser power. Yet a significant portion of the incident laser radiation is reflected from the diamond surfaces due to the high refractive index of diamond. For the CO<sub>2</sub> laser the loss is about 30% at an incident angle of 20°.

For the collection of the incandescent light for temperature measurement, *chromatic aberration* has to be considered. The problem is illustrated schematically in Figure 3. In the present case, spectra are measured between about 500 and 800 nm. For the microscope objectives used in previous experiments the change in the focal point position (chromatic aberration) over this wavelength range was large compared with the laser-heated spot, causing significant distortion of the emission spectrum and errors in the temperature measurements of the order of 1000 K. This was one of the major error sources in earlier experiments. Even a new achromatic lens that we tested recently, with a very small focal length of 6 mm (diameter 3 mm) and a chromatic aberration of the order of 10  $\mu\text{m}$  between 500 and 800 nm, resulted in a distortion of the emission spectra and temperature uncertainties of  $\pm 300$  K. The problem can

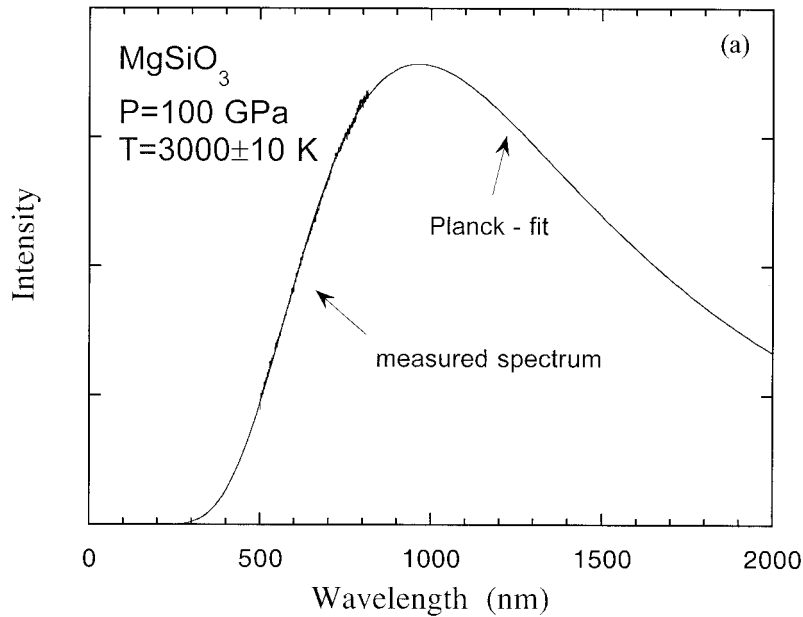


**Figure 4.** Two examples of temperature measurements at extreme conditions, showing the collected emission spectra and the Planck fits (and fitting error). (a)  $\text{MgSiO}_3$  is a low-emissivity material heated with a  $\text{CO}_2$  laser at 100 GPa. (b) SiC was heated with a  $\text{CO}_2$  laser to 6700 K, the highest temperature measured thus far in a diamond cell.

be circumvented by using mirror optics with zero chromatic aberration (shown schematically in Figure 1). Objectives with long focal lengths may be easily manufactured from aluminum-coated plano-convex and plano-concave lenses with radii ratios of about 2.62 [Kingslake, 1978].

## 2.7. Temperature Measurements

Once temperature gradients are minimized and the proper collecting optics are used, the measurement of temperature is remarkably straightforward and accurate. The mirror objective shown in Figure 1 produces an enlarged image of the laser-heated spot at the entrance of a monochromator. If the commonly used entrance slit is replaced with a pinhole, very small areas (equivalent to 1–3  $\mu\text{m}$  diameter) within this hot spot can be sampled, allowing accurate measurements of temperature gradients. Sampling from such small areas is especially important at very high pressures (above 100 GPa), where the dimensions of the pressure cell have to be reduced, leading to an increase in temperature gradients. In the earlier experiments this technique of point measurement was not used, and therefore peak temperatures could not be measured directly [Heinz and Jeanloz, 1987; Williams *et al.*, 1987]. The final temperature estimate required large corrections, and this may have been the other major source for systematic errors in those experiments.

The incandescent light is typically collected in a spectral range between 500 and 800 nm based on the sensitivity of the most commonly used Si array or *charge-coupled device (CCD)* detectors. The optical system is

calibrated with a light source (in general, a tungsten ribbon lamp) with known intensity versus wavelength distribution.

The Planck radiation function

$$I(\lambda) = \frac{\varepsilon c_1 \lambda^{-5}}{e^{c_2/\lambda T} - 1} \quad (1)$$

is used to calculate the temperature  $T$ , from the measured intensities  $I$ , at each wavelength  $\lambda$ .  $C_1$  and  $C_2$  are constants, and  $\varepsilon$  is the *emissivity*, which for a black body is 1 and for a gray body is less than 1. Here  $\varepsilon$  is wavelength dependent, but this dependence is only known for a limited number of materials (such as iron and tungsten) at ambient pressure and high temperature. For the temperature calculation,  $\varepsilon$ , in general, is taken as wavelength independent. At about 3000 K, temperatures are lowered by about 100 K if the wavelength dependence of iron or tungsten is included. The reliability of the temperature measurement can be tested by measuring the melting temperature of tungsten in vacuum using laser heating (see below). Sixteen measurements resulted in a melting temperature of  $3671 \pm 90$  K, compared with a literature value of 3680 K. Figure 4 shows two measured emission spectra and the associated Planck radiation function for two extreme cases: (1) at very high temperature and (2) for a material with low emissivity at very high pressure. For routine measurements the quality of the fits yields a precision and reproducibility of the order of  $\pm 10$  K, largely independent of pressure, temperature, or material.

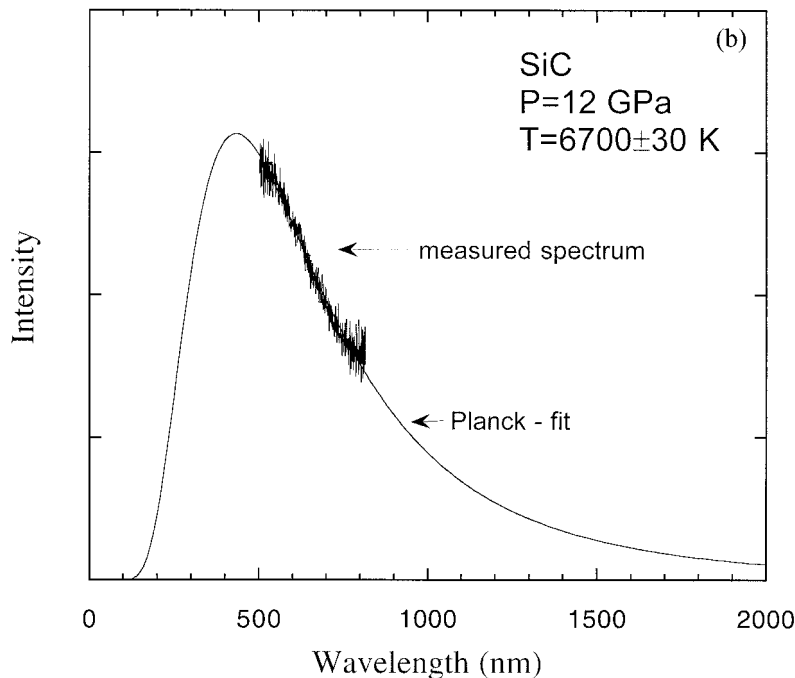


Figure 4. (continued)

## 2.8. Temperature Gradients

Temperature gradients can only be measured with the optical setup described above, which allows measurements from areas that are much smaller than the hot spot. It is important to characterize the temperature gradient for each experiment because they depend strongly on the cell (sample) geometry, temperature, and pressure and the type of laser. The requirements for different types of experiments vary. For example, for melting experiments on metals, where heating, melting, and temperature measurement occur at the sample sur-

face, only radial temperature gradients have to be considered. For phase equilibrium studies on transparent minerals using *Raman spectroscopy*, axial temperature gradients, which cannot be measured, can be minimized using very thin samples. In studies of high-temperature equations of state, or melting experiments using X rays, thicker samples are required. In these cases the difficulty is minimizing axial temperature gradients within the sample when temperatures are measured from the sample surface. Figure 5 shows a radial temperature profile of a metal surface heated with a YAG laser at 30 GPa in

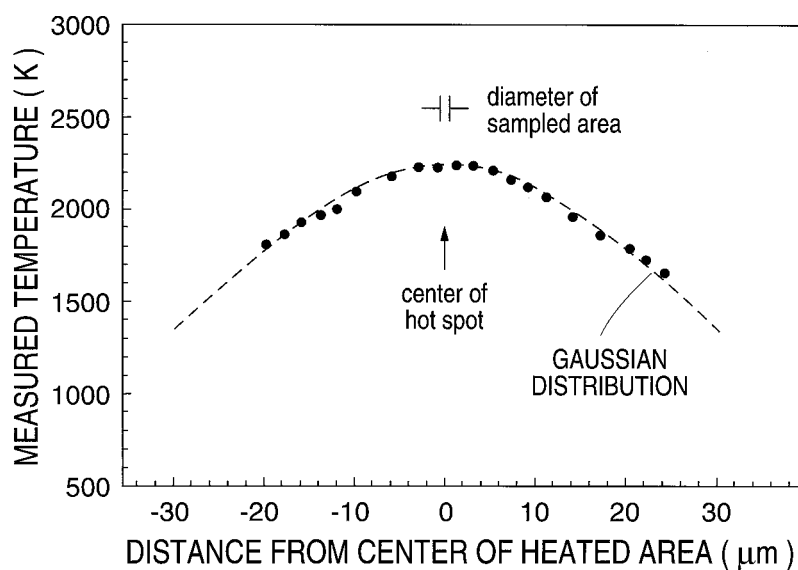
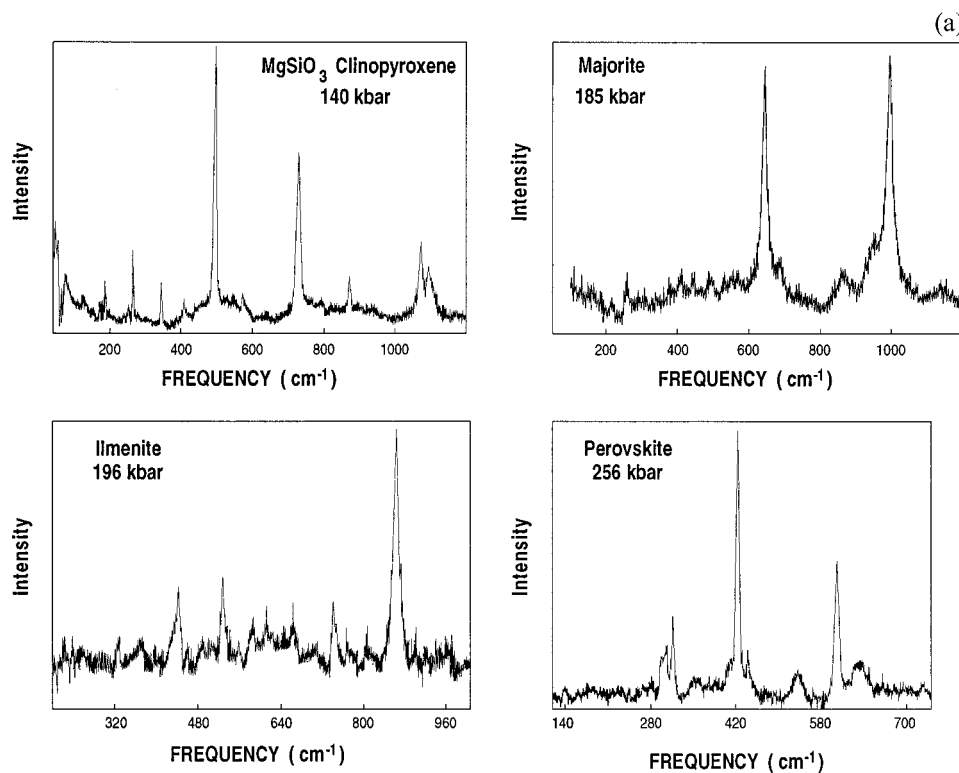


Figure 5. Temperature gradient of an iron foil heated at 30 GPa. Temperatures were measured from areas with  $1 \mu\text{m}$  in diameter.



**Figure 6.** (a) Examples of Raman spectra of four high-pressure polymorphs of  $\text{MgSiO}_3$  synthesized in the  $\text{CO}_2$  laser-heated diamond cell. Spectra are taken at high pressure, and the locations of the Raman frequencies are highly specific, allowing quick phase transition studies. (b) Example of phase identification after synthesizing  $(\text{Mg}, \text{Fe})\text{SiO}_3$ -perovskite from  $(\text{Mg}, \text{Fe})\text{O}$  and  $\text{SiO}_2$  at 100 GPa and 2800 K. Pressures are measured from ruby chips in the argon pressure medium.

an argon pressure medium. Temperature profiles in most experiments are less smooth, because surface texture and absorption may change due to phase transitions, recrystallization, melting, or chemical diffusion.

### 3. DETECTION OF PHASE TRANSITIONS IN THE DIAMOND CELL

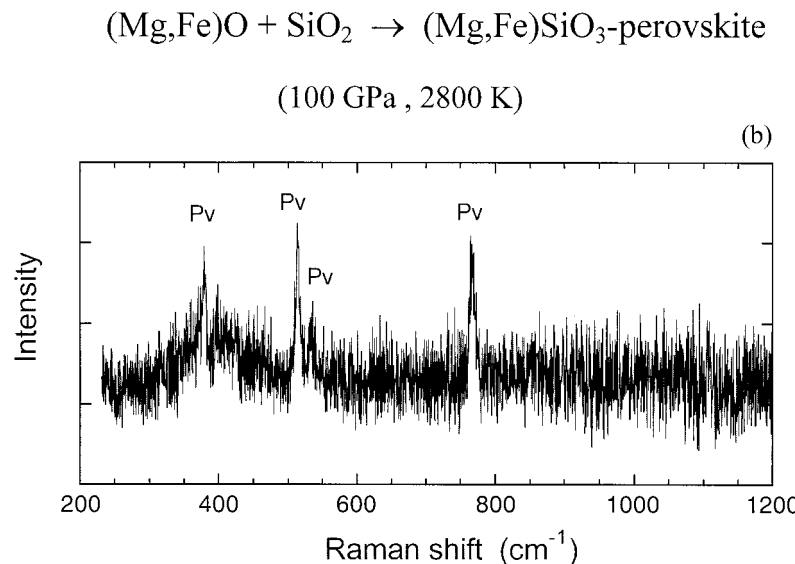
The diamond cell is a formidable tool for detecting high-pressure phase transitions using a variety of methods. In many cases the transitions can be observed visually by changes in color, texture, or shape, and refractive index. In the case of melting, motion is readily detectable.

#### 3.1. Solid-Solid Phase Transitions

For minerals the most reliable detection of phase transitions is by Raman and infrared spectroscopy. Raman is more advantageous because of higher spectral resolution and because measurements are possible on very small samples or portions thereof due to the small laser beam diameter. The spectra can be obtained on temperature-quenched samples while the sample is under pressure. Measurements at simultaneously high pressure and high temperature are possible but are very

difficult due to the incandescent radiation. From these samples at room temperature, sharp Raman bands can be measured within seconds on micron-sized crystals, which can be randomly shaped and oriented. Different high-pressure polymorphs of the same material have distinctly different spectra. This allows quick and accurate phase equilibrium studies (see below). Moreover, from the spectral shift of Raman bands with pressure, which have been measured for many major mantle polymorphs, a number of important thermodynamic properties, such as entropies, specific heats, and *Grüneisen parameters*, and even phase boundaries can be derived with high accuracy (see, for review, *Chopelas* [1999]). Figure 6 shows examples of spectra of three high-pressure polymorphs of  $\text{MgSiO}_3$  at high pressure.

Most phase boundaries of minerals relevant to the transition zone (about 15–25 GPa) have been measured in multianvil presses by the quench method: A sample, held at some pressure and temperature for some time, is temperature-quenched, and the sample is subsequently analyzed outside the pressure vessel in the metastable state. At the higher pressure end, lack of reliable calibrants reduces the accuracy in pressure and temperature. This can be demonstrated for the phase diagram of  $(\text{Mg}, \text{Fe})_2\text{SiO}_4$  (olivine), the most common mineral in the upper mantle: Measurements of the  $\alpha$ -to- $\beta$  transition,

**Figure 6.** (continued)

which is considered to be responsible for the 400-km seismic velocity discontinuity (about 13 GPa) and is used to derive the temperature at that depth, is observed at the same pressure and temperature conditions in both multianvil presses and laser-heated diamond cells [Boehler and Chopelas, 1992; Katsura and Ito, 1989]. For (Mg<sub>0.88</sub>Fe<sub>0.12</sub>)<sub>2</sub>SiO<sub>4</sub> the transition is at 1850 ± 50 K at 13 GPa. However, there is considerable disagreement for the transition of  $\gamma$ -(Mg,Fe)<sub>2</sub>SiO<sub>4</sub> (Ringwoodite) to a (Mg,Fe)SiO<sub>3</sub>-perovskite-(Mg,Fe)O-magnesiowüstite assemblage, thought to be responsible for the seismic discontinuity at 660 km depth (23.8 GPa). Compared with the  $\alpha$ -to- $\beta$  transition, this transition pressure is less sensitive to temperature, which reduces the accuracy in temperature estimates at that depth, but it is also much less sensitive to the iron content, within the range of iron contents relevant to the Earth's mantle [Ito and Takahashi, 1989]. For the iron-free end-member this transition has been measured in the laser-heated diamond cell in the temperature range 1600–2800 K [Boehler and Chopelas, 1992]. At 23.8 ± 0.2 GPa, a transition temperature of 1900 ± 100 K was found, which is higher but in reasonable agreement with previous multianvil work [Ito and Takahashi, 1989]. However, more recent in situ multianvil X-ray measurements [Irifune, 1998] imply a mantle temperature about 1000 K lower than the one commonly accepted. This discrepancy deserves further investigation. Most likely, more reliable  $P$ - $T$  calibrants have to be found for multianvil measurements. For example, thermocouples show large pressure effects on their voltage-temperature relationships even at low pressure (3.5 GPa) [Getting and Kennedy, 1970]. These effects, which may be significant at pressures above 20 GPa, have been ignored in the estimates of temperature uncertainties in multianvil work. Pressures have been determined by extrapolation from known transitions in the 15-GPa range. In multianvil X-ray studies, pressures

are derived from an assumed high-temperature equation of state of a calibrant (for example, NaCl) and the temperature, both of which are not accurately known.

An important advantage of the diamond cell is that phase boundaries can be measured over a much larger temperature range, thus improving estimates on their slopes. Reverse transitions may also be measured more easily due to in situ phase identification. The main disadvantage of the diamond cell is that because of the small sample dimensions, multicomponent systems are hard to study, unless the starting material is a homogeneous glass (see below).

### 3.2. Diamond Cell Melting Experiments

Melting can be detected in situ for most materials by several methods: (1) by measurement of discontinuous changes of the absorption of the laser radiation, (2) by detection of changes in the reflectivity of the sample at a wavelength different from that of the heating laser, and (3) by direct visual observation of melting on the sample surface. For direct visual observation the heated sample is illuminated with a blue argon laser beam, which produces a laser-speckle pattern on the surface of the sample. When the material melts, motion on the surface can be easily observed. Melting temperatures can then be reproducibly measured by temperature cycling through melting and freezing with a precision of about 100 K. Solid-solid phase transition may also be observed by this method, but the changes on the sample surface are much less obvious.

Samples are heated either directly, by direct absorption of the laser radiation, or indirectly, if their absorption is low at either laser wavelength (1 or 10  $\mu$ m). In that case, the sample is heated in contact with an absorbing metal that does not react with the sample. As soon as the heated metal surface reaches the melting temperature of the sample, melting can be observed by

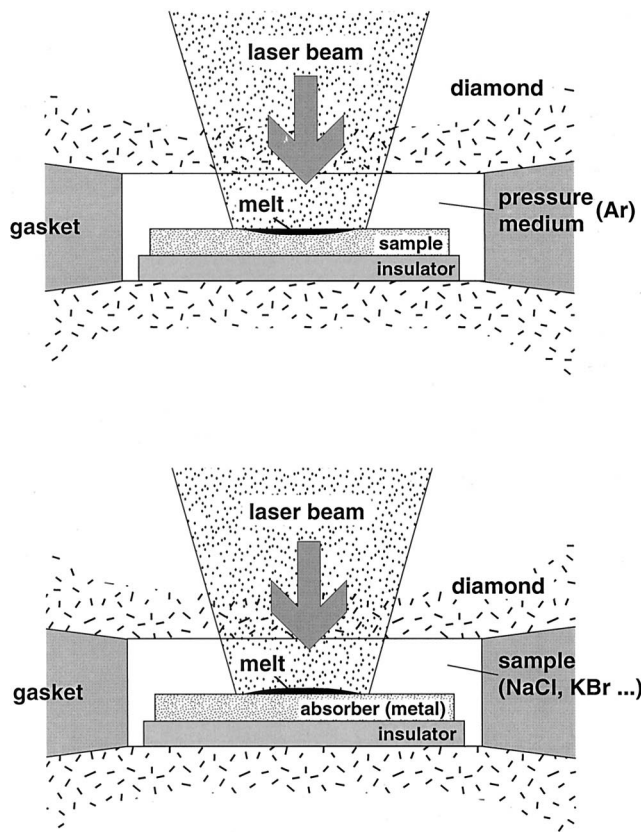


**Figure 7.** Schematics of melting of materials with high laser absorption (metal, upper panel) and materials with low absorption (for example, alkali halide, lower panel), using a metal absorber with higher melting temperature. The onset of melting is monitored by the change in optical properties (laser absorption or reflectivity) or by in situ visual observation of changes in the surface texture, made visible with blue argon-laser radiation.

changes in the refractive index or by changes in its absorption properties. This is illustrated in Figure 7, which shows both cases, direct and indirect heating. Both cases may be used in the same experiment. For example, if iron is embedded in an argon pressure medium, both melting temperatures can be observed in one temperature cycle, even though the signal from argon is significantly weaker than that from the metal [Jephcoat and Besedin, 1996].

Melting and phase transitions may be detected by *in situ* X-ray diffraction, but this is far more complicated than optical methods because of the need for synchrotron radiation and strict requirements on the pressure medium, temperature gradients, and crystallinity of the sample. During laser heating, crystal size may change significantly when the sample undergoes phase transitions and melting. For *powder diffraction*, micron-sized crystals have to be statistically orientated, or the sample has to be rotated, which is difficult to do during laser heating. These problems may be circumvented by increasing the sample size and the cross section of the

X-ray beam. This, however, requires larger diamond flats, resulting in a reduction of the pressure range. Additionally, larger samples result in larger temperature gradients because of limited laser power. Moreover, for metals the absorption of the laser radiation and the temperature measurement occur at the sample surface. Because this surface is always hotter than the interior of the X-rayed sample, melting temperatures will be overestimated. Another complication is that loss of X-ray pattern may be due to other processes besides melting, such as recrystallization or an increase in the defect concentration. It is therefore important to check agreement between melting and freezing temperatures and to directly compare optical and X-ray methods. The essential requirement for uniform sample temperatures is the use of a thermally insulating pressure medium. Noble gases and alkali halides are best suited for this purpose, but their X-ray patterns often overlap with that of the sample.

#### 4. MELTING TEMPERATURES, HIGH-PRESSURE PHASES OF IRON, AND THE TEMPERATURE IN THE CORE

One of the major constraints of the temperature in the center of the Earth is the melting temperature of iron at the pressure conditions of the inner core boundary (about 330 GPa, or 3.3 Mbar). Because the melting temperature of iron cannot be measured at this pressure by any method, it is important to determine the pressure dependence of melting over a large pressure range and use this information for extrapolation. Theoretical estimates of melting temperatures and *molecular dynamics simulations* may be accurate for simple materials such as noble gases when other thermodynamic data are available [Belonosko, 1997; Boehler *et al.*, 1997; Zha *et al.*, 1986], but they have yielded very large variations for geological materials, including iron. The main reason is that these materials have complicated phase diagrams, as well as complicated electronic and bonding structures. Moreover, estimates of the core temperature depend on our knowledge of the effect of lighter elements that are required based on the density deficit in the core. The density of the core, derived from seismic measurements, is about 8% less than the density of pure iron obtained from theory or high-pressure measurements (see below). The nature of such light elements has been a matter of speculation, the most favored candidates being sulfur and oxygen.

The last few years have yielded agreement in melting temperatures of iron measured under static pressure conditions in the diamond cell among the laboratories that have been involved in this research using state-of-the-art temperature measurements (Geophysical Laboratory, Livermore, Mainz, and Uppsala). At 100 GPa the melting temperature is well constrained between 2700 and 3000 K, and the melting curve to 200 GPa [Boehler,

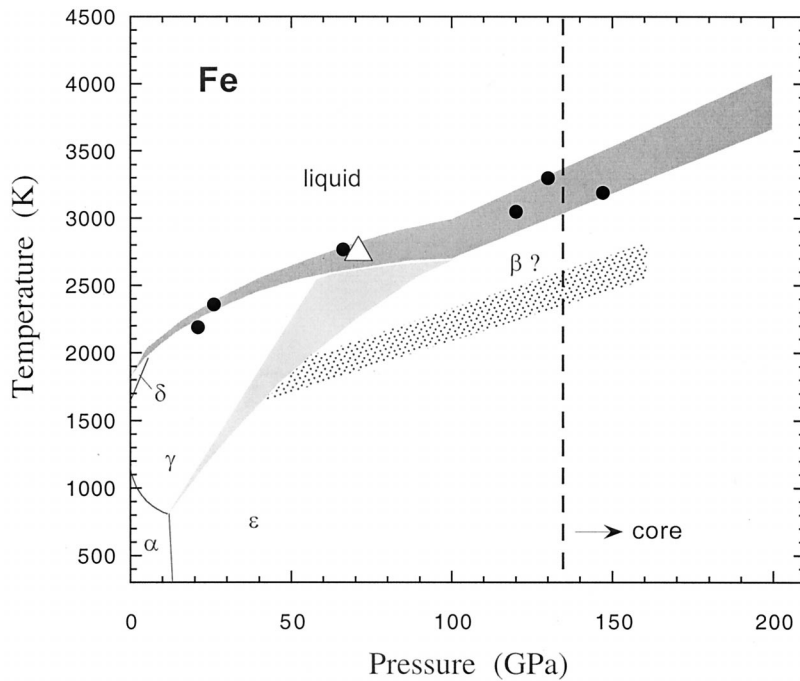


**Figure 8.** Phase diagram of iron from diamond cell experiments. The melting band (darker shading) contains data to 40 GPa [Yoo *et al.*, 1992], 50 GPa [Yoo *et al.*, 1996], 75 GPa [Shen *et al.*, 1998] (except their highest-pressure data point), 150 GPa [Saxena *et al.*, 1994], and 200 GPa [Boehler, 1993], including a new shock melting point of preheated iron at 71 GPa (triangle) [Ahrens *et al.*, 2000] and the latest measurements (dots) using modified techniques (see text). The location of the  $\gamma$ - $\epsilon$  phase boundary (lighter shading) shows significant uncertainty. The existence of a new high pressure ( $\beta$ ) is still under debate.

1993] was measured using the same state-of-the-art methods. A variety of detection methods have been used: direct visual observation of motion during melting, change in sample reflectivity, discontinuity in the laser power–temperature function, melt-related changes on the sample surface, and loss of X-ray diffraction lines. Figure 8 shows the pressure and temperature range in which melting of iron has been measured in the diamond cell by these groups. The band in Figure 8 representing the melting curve is taken from Boehler's [1993] measurements to 200 GPa, which shows an uncertainty of about  $\pm 200$  K at the highest pressures. This band covers all data from all other recent studies taken up to 150 GPa [Saxena *et al.*, 1994; Shen *et al.*, 1998; Yoo *et al.*, 1992, 1996]. The temperature uncertainties also include corrections due to the wavelength dependence of the emissivity of the order of 200 K [Boehler, 1993; Saxena *et al.*, 1994]. One single data point from recent X-ray measurements to 75 GPa [Shen *et al.*, 1998] falls 100–200 K outside this band, but this could be easily explained by temperature gradients, which cause an overestimate in the melting temperature, as described earlier. New shock sound velocity measurements on preheated iron yield a melting temperature at 71 GPa that is also in excellent agreement with the static data [Ahrens *et al.*, 2000].

Figure 8 also shows the solid phase diagram of iron. There is consensus below 50 GPa on the phase bound-

aries between  $\alpha$  (bcc),  $\gamma$  (fcc),  $\delta$  (bcc), and  $\epsilon$  (hcp). There is, however, considerable variation in the maximum stability pressure of  $\gamma$ -iron and therefore the location of the  $\gamma$ - $\epsilon$ -liquid triple point. Knowledge of its location is important because it is the starting point of the most important branch of the iron melting curve, used for extrapolation to inner core pressures. This triple point has been subject to much debate before intensive investigation of the iron phase diagram placed it between 50 and 100 GPa. For example, estimates on its location in 1986 ranged from 75 GPa [Boehler, 1986] to 280 GPa [Anderson, 1986]. Recent X-ray studies [Shen *et al.*, 1998] place this triple point near 60 GPa and 2700 K, but the new shock data on preheated iron [Ahrens *et al.*, 2000] reveal no evidence of this phase change up to 71 GPa. New X-ray diffraction work on the  $\gamma$ - $\epsilon$  transition [Dubrovinsky *et al.*, 1998] also suggests a higher pressure of this triple point than that reported by Shen *et al.*. Placing this triple point somewhere between 70 and 100 GPa is in agreement with the melting curve shown in Figure 8.

#### 4.1. Is There a New High-Pressure Phase of Iron?

Geophysical, theoretical, and experimental issues are associated with this question. Knowledge of the structure of solid iron in the inner core is required for the interpretation of the seismically observed anisotropy and the inner core transition zone [Song and Helmberger,

1998], and in free energy calculations in order to estimate the energy release upon the freezing at the inner core boundary [Anderson, 1993]. The importance of these issues may be debated because anisotropy in the core may have a number of reasons, and energy differences of close-packed high-pressure phases of iron may be insignificant, but knowledge of the structure is certainly important in molecular dynamics simulations.

Whether or not there is another high-pressure phase of iron is important, however, for the interpretation of shock data. The termination of the  $\gamma$  phase below 100 GPa requires a new phase [Boehler, 1986] in order to reconcile the solid-solid transition observed at 200 GPa by shock-velocity measurements [Brown and McQueen, 1986] (see below). Indeed, changes in the optical properties of iron observed in laser-heated diamond cell experiments suggested such a transition [Boehler, 1993; Saxena et al., 1993]. Further X-ray studies, however, were controversial, showing transformations from  $\epsilon$ -iron (hcp) to an orthorhombic phase [Andrault et al., 1997], or to dhcp [Saxena et al., 1996a; Yoo et al., 1996], or, in a more recent study no transition, indicating that hcp iron is the stable phase [Shen et al., 1998]. The reason for this discrepancy is not yet clear, but in addition to differences in the heating techniques and X-ray detection methods used in these studies, there may be an additional error source: Both the observed distortion from hcp to orthorhombic and a change in stacking order hcp  $\rightarrow$  dhcp are only very minor structural changes. In all these experiments solid, high-strength pressure media were used, and there is a strong possibility that the observed phase transitions are due to nonhydrostatic stresses. In any case, it is important to point out that both results, phase transition or not, present a serious problem in the interpretation of the shock transition found at 200 GPa, as explained in the next section.

#### 4.2. Shock Melting of Iron

Shock wave experiments are the only way to achieve the pressure and temperature conditions of the inner core boundary. These experiments yield accurate pressure-density relationships along a nearly isentropic pressure-temperature path (Hugoniot). The measurement of melting has several problems. First, Hugoniot temperatures rise more rapidly than the melting temperature: For iron, at present, it is not clear at exactly what pressure the Hugoniot crosses the melting curve (see below). Indications for melting are (1) discontinuities in the measured volumes (extremely small, but they have been reported [Anderson and Duba, 1997]), (2) discontinuities in temperatures [Williams et al., 1987; Yoo et al., 1993], or (3) discontinuities in sound velocities [Ahrens et al., 2000; Brown and McQueen, 1986; Nguyen and Holmes, 1998]. The estimate of the melting temperature at 330 GPa then requires an extrapolation using a Lindemann melting relation [Anderson and Duba, 1997] or other empirical melting relations, as, for example, a

linear extrapolation of the melting temperature versus volume [Kraut and Kennedy, 1966]. The second difficulty in shock experiments is the determination of the temperature. Thermodynamic calculations [Boness and Brown, 1990; Brown and McQueen, 1986] depend on estimates on the specific heat and Grüneisen parameter, which for iron lead to uncertainties of the order of  $\pm 500$  K. Direct temperature measurements are subject to large uncertainties due to the small timescale and the unknown thermal and optical properties of the window material through which the iron surface is observed. Thermal conduction changes this surface temperature in a complicated time-dependent way [Gallagher et al., 1993; Yoo et al., 1993], resulting in temperature corrections of the order of 1000 K. Other issues are overshoot of the melting temperature due to the small timescale in shock experiments and the exact estimate of the melting pressure, both of which will be discussed below.

Five data sets exist on shock melting of iron [Ahrens et al., 2000; Brown and McQueen, 1986; Nguyen and Holmes, 1998; Williams et al., 1987; Yoo et al., 1993]. Brown and McQueen [1986] measured sound velocities up to 400 GPa and observed two discontinuities, one at 200 GPa, interpreted as the  $\epsilon$ - $\gamma$  transition, and one at the transition to liquid iron at 240 GPa. Hugoniot temperatures were calculated, and the range of estimates is shown in Figure 9. Subsequent direct temperature measurements [Williams et al., 1987] have recently been corrected downward in temperature, and the number of data points has been reduced to four [Ahrens et al., 2000; Gallagher et al., 1993], all of which lie on a straight line within the Hugoniot temperatures calculated by Brown and McQueen. These four data points give no indication of any phase transition, and they are not plotted in Figure 9, for simplification. The second data set on measured shock temperatures [Yoo et al., 1993] shows discontinuous behavior above about 250 GPa, which has been interpreted as being due to melting. However, below melting, the data lie over 1000 K above the calculated Hugoniot temperatures. Recently, new sound velocity data of iron between about 190 and 320 GPa have been reported [Nguyen and Holmes, 1998]. These data, in contrast to the Brown and McQueen data, show only one drop in sound velocity (a total of about 12% from solid to liquid), starting at 220 GPa. No solid-solid transition was observed. This difference is under debate, different sample purities being a possible cause. In summary, the exact pressure temperature at which iron melts during shock compression is uncertain.

The role of overshoot of the melting curve in shock experiments also is not clear: Although overshoot of about 1000 K has been observed in a number of experiments on silicates and alkali halides [Boness and Brown, 1993; Lyzenga et al., 1983], recent shock measurements of sound velocities of preheated iron [Ahrens et al., 2000] do not show such an overshoot, and the estimated melting temperature at 71 GPa is in excellent agreement with the static data. Moreover, it has been shown in recent

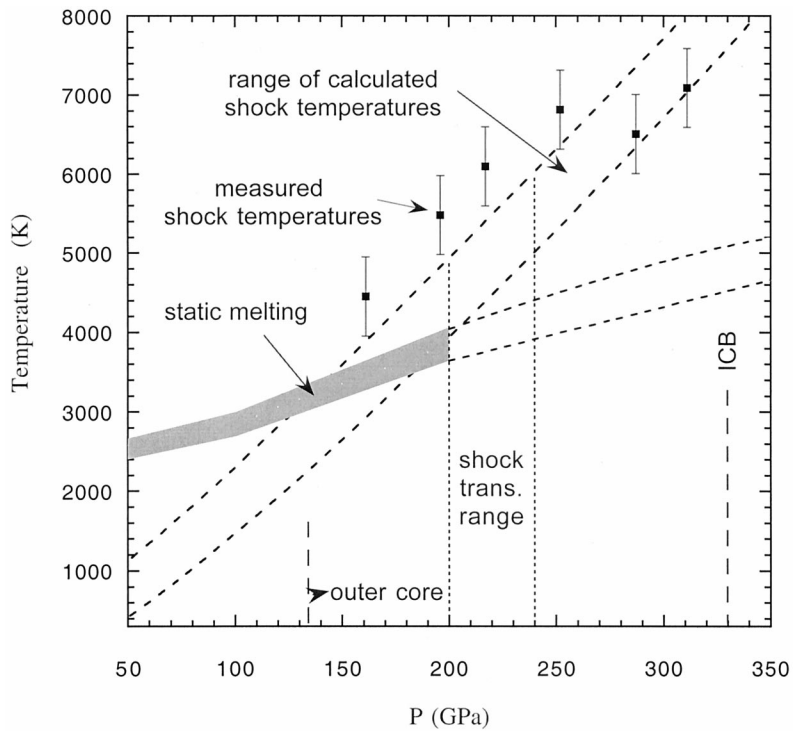


**Figure 9.** Shock temperatures of iron, calculated from thermodynamics [Brown and McQueen, 1986] and measured [Yoo et al., 1993]. The band of calculated temperatures also includes four data points by Ahrens et al. [2000] and Gallagher et al. [1993]. Three discontinuities were reported in the shock-velocity measurements between 200 and 240 GPa [Brown and McQueen, 1986; Nguyen and Holmes, 1998]. The melting temperatures from diamond cell measurements are shown for comparison.

diamond cell melting measurements of alkali halides [Boehler et al., 1996; Boehler et al., 1997] and aluminum [Boehler and Ross, 1997] for which the pressure ranges in the static and shock experiments overlap that, in general, the results are in good agreement. Iron seems to be the only material for which such an agreement is lacking, with a discrepancy of over 1000 K at 240 GPa.

There are two possible ways to reconcile static and shock experiments: a reinterpretation of the shock data or the addition of an additional triple point between 200 and 240 GPa, which would deflect the melting curve upward. The latter possibility has been suggested by Anderson and Duba [1997]. A triple point between 200 and 240 GPa, however, could only be due to a phase change from one close-packed phase to another. Such a minor structural transition would be unlikely to cause the strong increase in the melting slope required to satisfy both static and shock experiments. For example, at around 100 GPa ( $\gamma$ -e-liquid-triple point), the melt slope changes from about 4 to 10 K GPa<sup>-1</sup>. A triple point at 200 GPa would have to have a further change from about 10 to over 35 K GPa<sup>-1</sup>, and this is highly unlikely due to the very small volume change of such a transition.

The second possibility is reinterpreting the shock data. Because the measured shock temperatures for solid iron [Yoo et al., 1993] lie considerably above the calculated shock temperatures, this data set will be dis-

regarded for the present discussion, which leaves only the shock-velocity measurements [Brown and McQueen, 1986; Nguyen and Holmes, 1998]. In the Brown and McQueen data, both the solid-solid and melt transitions have a drop in sound velocity of about 5%. This is suspicious for two reasons. First, if the first drop were due to a phase transition between close-packed cubic structures, as has been observed by some X-ray measurements described above [Andrault et al., 1997; Saxena et al., 1996a], it is unlikely that such a phase transition would have as great a velocity change as a transition from solid to liquid. Second, for a number of other metals the velocity jump at melting is close to 10% [Boehler and Ross, 1997]. The shock measurements of sound velocities of preheated iron [Ahrens et al., 2000] yield a drop in sound velocity at 71 GPa of about 12%. It is highly unlikely that this velocity change decreases to 5% at 240 GPa. For these reasons, and in view of the newer data [Nguyen and Holmes, 1998], one may argue that in the shock experiment melting starts between 200 and 220 GPa, as indicated in Figure 10, and the region between 200 and 250 GPa represents a region of mixed states in the shock. The total change in sound velocity would then be about 10%, which is closer to the value of the other metals studied. If shock melting occurs near 200 GPa, diamond cell work and the shock work can be brought into close agreement, as is evident from Figure 9, with a melting temperature near 4000 K at 200 GPa.

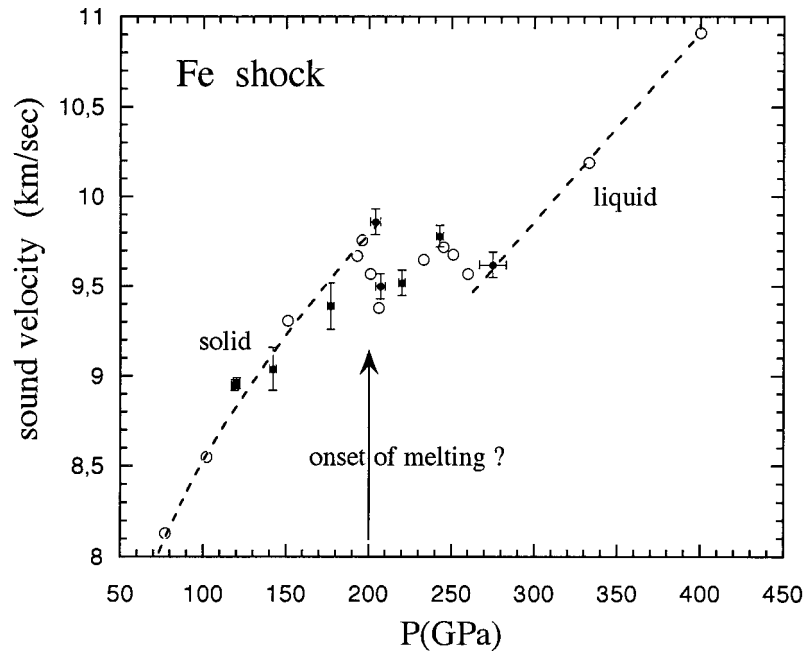


**Figure 10.** Shock sound velocity data [Brown and McQueen, 1986] using explosives (solid symbols) and a two-stage gas gun (open symbols). If the onset of melting is at 200 GPa instead of the reported 240 GPa, static and shock melting of iron can be brought into agreement.

#### 4.3. Temperature at the Inner Core Boundary (330 GPa): Extrapolation of the Iron Melting Curve

There is a very good consensus in all recent iron melting experiments [Ahrens *et al.*, 2000; Boehler, 1993; Saxena *et al.*, 1994; Shen *et al.*, 1998; Yoo *et al.*, 1992] that the upper bound of the melting temperature at 100 GPa is 3000 K. Using this temperature as a starting point yields significantly different melting temperatures at 330 GPa if static or shock data are used. A case can be made, however, for the static data to 200 GPa [Boehler, 1993] if one assumes that a Lindemann equation adequately describes melting behavior at high pressure. This equation can be expressed as

$$\frac{d \ln T_m}{d \ln \rho} = 2(\gamma - \frac{1}{3}), \quad (2)$$

where  $T_m$  is the melting temperature,  $\rho$  is the density, and  $\gamma$  is the Grüneisen parameter. For many materials this equation has been shown to well describe melting at high pressure, but it should still be applied with caution to predict and extrapolate melting data because in many other cases it has proved inadequate. Moreover, the value of  $\gamma$  at the pressure and temperature conditions of the Earth's interior is not known well enough to derive melting temperatures.

As an approximation, the density dependence of  $\gamma$  may be written as

$$\frac{\gamma}{\gamma_0} = \left( \frac{\rho_0}{\rho} \right)^q, \quad (3)$$

or  $\gamma\rho = \text{const}$ , for  $q = 1$ . Subscript zero is for zero pressure. Measurements of the pressure dependence of  $\gamma$  for a large class of materials have shown that  $q$  clusters

around 1 [Boehler and Ramakrishnan, 1980], with an uncertainty of about 30%. However,  $\gamma$  is temperature dependent and changes across phase transitions [Ramakrishnan *et al.*, 1979], and  $q$  seems to decrease with pressure [Boehler and Young, 1984]. Using (3) with  $\gamma_0 = 2.44$  for liquid iron [Stevenson, 1981] yields  $\gamma = 1.5$  at 150 GPa (at about 40% compression). This agrees with a value of  $1.6 \pm 0.3$  obtained from new shock results on preheated iron at 71 GPa [Ahrens *et al.*, 2000] and with the theoretical estimate of  $1.7 \pm 0.3$  at 150 GPa by Stevenson [1981]. Thus values of  $\gamma$  for iron for core pressures most likely range between about 1.4 and 1.7. The melting curve measured in the diamond cell between 100 and 200 GPa results in an average value of  $\gamma = 1.45 \pm 0.3$  using (2). In contrast, connecting a melting line between the well-accepted melting temperature at 100 GPa of 3000 K to Brown and McQueen's [1986] 5500 K at 240 GPa yields a high value of  $\gamma = 2.2$ .

The static results between 100 and 200 GPa may also be extrapolated using an empirically derived linear relationship between the melting temperature and the density [Kraut and Kennedy, 1966]. Both relationships yield a melting temperature at 330 GPa of  $4850 \pm 200$  K [Boehler, 1993], about 1000 K lower than when using Brown and McQueen's [1986] shock data.

In summary, it is difficult to reconcile estimated melting temperatures of iron at the inner core boundary from static and shock melting experiments unless high values of the Grüneisen parameter or an additional triple point with a very large change in the melting slope are assumed. The best solution to reconcile both data sets is to put the shock melting pressure at 200 instead of 240 GPa with a melting temperature near 4000 K. Extrapol-

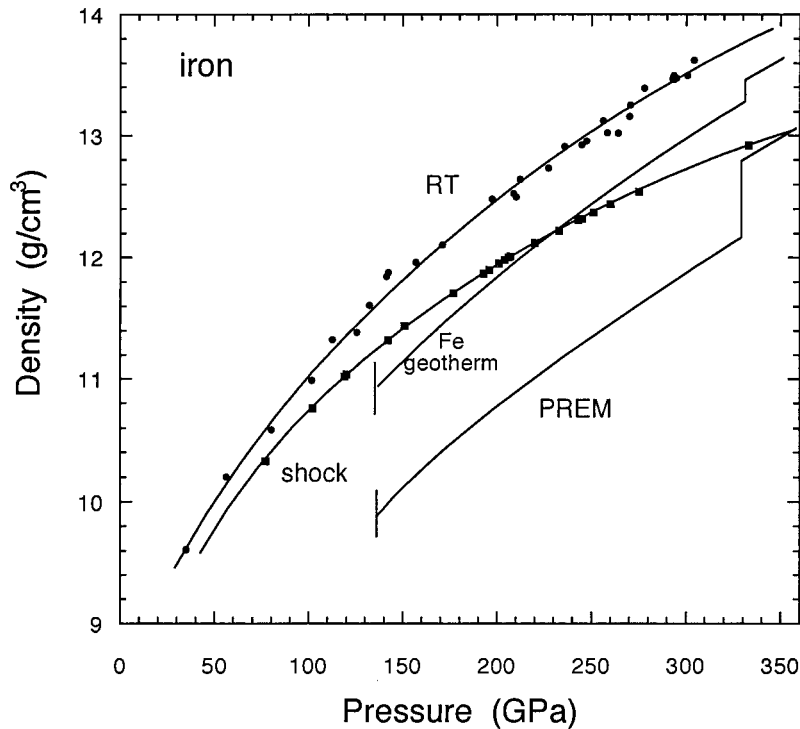


**Figure 11.** Densities of iron in comparison with seismically derived core densities (preliminary reference Earth model [Dziewonski and Anderson, 1981]). Room temperature measurements are from diamond cell work [Mao et al., 1990]. Shock densities along an isentrope are from Brown and McQueen [1986]. The density of pure iron along a geotherm is calculated from the room temperature density and taking a thermal expansion coefficient  $\alpha = 1/V_0(dV/dT)_T = \alpha_0(V/V_0)^5$  (see text and Table 1). The volume change of melting is assumed to be 1%. Density error bars of 2% are shown. The density difference between liquid iron and the outer core is 9% and is 5% for solid iron and the inner core.

olation of the melting curve between 100 and 200 GPa to the inner core boundary pressure (330 GPa) using a linear pressure-melting temperature relationship, a Lindemann or a Kraut-Kennedy relationship yields a melting temperature of pure iron in the vicinity of 5000 K.

#### 4.4. Light Elements and the Density Deficit in the Core

A certain amount of light elements is needed in the outer core in order to match sound velocities or densities estimated for iron at outer core pressures with those derived from seismic data. The effect of Ni on the density of iron is negligible [Mao et al., 1990]. The key issues under debate are their nature, their amount, and their effect on the melting temperature of pure iron. The main constraints on the nature of these elements are cosmochemical abundance and relative volatility, and they have to be able to partition into iron during core formation. It is possible that several light elements are involved, which complicates the problem. A large amount of work on this subject has been published, providing cosmochemical constraints [e.g., Dreibus and Palme, 1996], experimental constraints on solubility of candidate light elements at low pressure [O'Neill et al., 1998] and high pressure [Hillgren and Boehler, 1998, 2000], and constraints from the density deficit in the core

[Poirier, 1994; Stevenson, 1981]. The most likely candidates are oxygen, sulfur, silicon, carbon, and hydrogen, but there is still a large uncertainty in any prediction.

The exact amount and nature of light elements required are not known because of uncertainties in both the seismically derived core density and the density of pure liquid iron at the pressure and temperature conditions of the core. The density of iron can be derived from the room temperature compression data measured to 300 GPa [Mao et al., 1990] and the *thermal expansion coefficient*  $\alpha$ . The pressure dependence of  $\alpha$  may be expressed as

$$\frac{\alpha}{\alpha_0} = \left( \frac{V}{V_0} \right)^n, \quad (4)$$

which was derived empirically [Chopelas and Boehler, 1992] with  $n$  ranging between 5 and 6. Calculating densities along the shock Hugoniot from Mao et al.'s room temperature densities and the above equation using  $n = 5$  yields excellent agreement with the measured shock densities of Brown and McQueen [1986]. Temperatures in the outer core ranging from 4000 to 4900 K and an assumed density decrease due to melting of 1% then yield the iron densities plotted in Figure 11 together with the room temperature isotherm, shock densities along the Hugoniot [Brown and McQueen, 1986], and preliminary reference Earth model (PREM) densities [Dzie-

**TABLE 1.** Properties of Iron in the Earth's Core

$P$ , GPa	$T$ , K	$\rho_0/\rho$ , <sup>a</sup> room temperature	$\alpha = \alpha_0(\rho_0/\rho)^5$ , $10^{-6} K^{-1}$	$\rho_{Fe(P,T)}$ , <sup>c</sup> g cm <sup>-3</sup>	$\rho_{PREM}$ , <sup>d</sup> g cm <sup>-3</sup>	$\gamma = \gamma_0(\rho_0/\rho)^{0.6}$ , <sup>e</sup> d	$\gamma_{Lindemann}$ , <sup>e</sup> e	$\gamma_{shock}$ , <sup>f</sup> f
135	4000	0.675	14	10.93 (liquid) <sup>g</sup>	9.90	1.34	1.45	
200	4300	0.630	9.9	11.86 (liquid) <sup>g</sup>	10.78	1.29		
240	4485	0.609	8.4	12.34 (liquid) <sup>g</sup>	11.24	1.26		
330	4900	0.570	6.0	13.28 (liquid) <sup>g</sup>	12.17 <sup>h</sup>	1.21		1.4
				13.42 (solid) <sup>g</sup>	12.76 <sup>i</sup>			

<sup>a</sup>From Mao *et al.* [1990].<sup>b</sup>Here  $\alpha_0 = 1.0 \times 10^{-4} K^{-1}$  (average from room temperature to  $T_m$ ). Equation is from Chopedas and Boehler [1992].<sup>c</sup>From  $\rho$ ,  $\alpha$ , and  $\Delta T$ .<sup>d</sup>From Ramakrishnan *et al.* [1978];  $\gamma_0 = 1.7$ .<sup>e</sup>From Lindemann equation (2) and melting slope between 100 and 200 GPa [Boehler, 1993].<sup>f</sup>From Anderson and Ahrens [1994].<sup>g</sup>Assuming  $\Delta\rho_{\text{melting}} = -1\%$ .<sup>h</sup>Outer core.<sup>i</sup>Inner core.

wonski and Anderson, 1981]. Key parameters are listed in Table 1. The density of liquid iron in the outer core is about 9% ( $\pm \sim 2\%$ ) higher than the seismic (PREM) density, and in the inner core it is about 5% higher. Addition of 8–10% oxygen or sulfur has been frequently adopted to make up the density deficit in the outer core. With regard to the uncertainty in this estimate one should keep in mind that the different seismically derived model densities for the core vary by as much as 2%, and the calculation of the density of pure iron along a geotherm may be uncertain by the same amount. A lowering of the required amount of light elements in the core is a consideration in view of new theoretical, cosmochemical, and experimental aspects. Recent theoretical estimates on the mixing volume in the iron-sulfur system predict a reduction of previous estimates of the amount of the required light element or elements [Sherman, 1997]. Cosmochemical arguments on volatility of sulfur [Dreibus and Palme, 1996] limit the sulfur content of the core to less than 6 wt %. New high-pressure measurement of the solubility of oxygen and silicon in liquid iron show that their solubilities are limited to a few percent at the  $P$ - $T$  conditions of the core-mantle boundary (130 GPa, 4000 K) [Hillgren and Boehler, 1998, 2000].

Estimates of the amount of light elements in the inner core are equally uncertain. Although the density difference  $\Delta\rho$  between the inner and outer core is well constrained from seismic data (0.5 g cm<sup>-3</sup>, or 4–5%) [Masters and Shearer, 1990], the exact value of  $\Delta\rho$  between solid and liquid iron is not. A direct estimate of  $\Delta\rho$  of melting from Hugoniot data is difficult and highly uncertain. Anderson and Duba [1997] estimate a value of about 0.3 g cm<sup>-3</sup>, which yields a ratio of light elements between the outer and inner core of about 4:1. Sherman [1995] estimates possible sulfur contents in the outer and inner core from the equations of state of iron and Fe<sub>3</sub>S and the density of the core. For example, if the outer core contains 6 wt % sulfur, an inner core made of pure iron would satisfy the density difference between the inner and outer core, but this solution is slightly outside the error bars shown in Figure 11.

#### 4.5. Effect of Light Elements on the Melting Temperature of Iron

The effect of light elements on the melting temperature of pure iron is fundamental for estimates of the core temperature. The melting depression can be determined experimentally or calculated from thermodynamics, but for core pressures both estimates lead to large uncertainties. Most previous estimates are based on measurements at low pressure, where the largest eutectic melting depression due to a combination of nickel, oxygen, and sulfur is about 700 K [Urakawa *et al.*, 1987; Usselman, 1975]. Theoretical estimates at core conditions require estimates of the melting temperature, the entropy of melting, the chemical potentials, and the concentration of light elements and yield values ranging from 600 to 1100 K [Anderson and Duba, 1997; Stevenson, 1981]. In these calculations, lower melting temperatures of iron and lower concentrations of light elements will decrease the melt depressions but most likely not eliminate them. Moreover, the relatively large density difference between the outer and inner core requires a change in chemical composition, and this is most likely a result of a eutectic-type system.

Only few measurements at very high pressure exist on the effect of oxygen and sulfur on the melting temperature of iron [Boehler, 1993, 1996a]. The in situ detection of the solidus in the diamond cell is much more difficult than detecting melting of a single phase, because for compositions that differ from the eutectic composition the small melt fraction at the eutectic temperature in a multicomponent system is hard to detect, and thus the *solidus temperature* may be overestimated using conventional optical methods. Therefore the more sensitive method for in situ sample observation of using the interference pattern created by an argon ion laser was used. Discontinuous changes in this interference pattern at the onset of melting were observed at temperatures that accurately agree with the solidus temperatures measured at low pressures using differential thermal analysis (DTA) for both the Fe-FeO and Fe-FeS systems.

We recently developed a new method for the accurate measurement of eutectic temperatures in the diamond

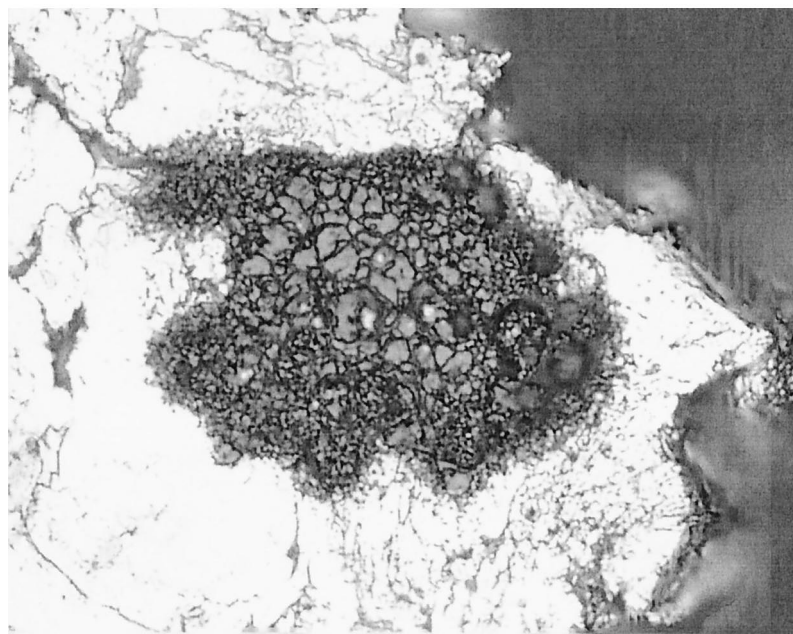
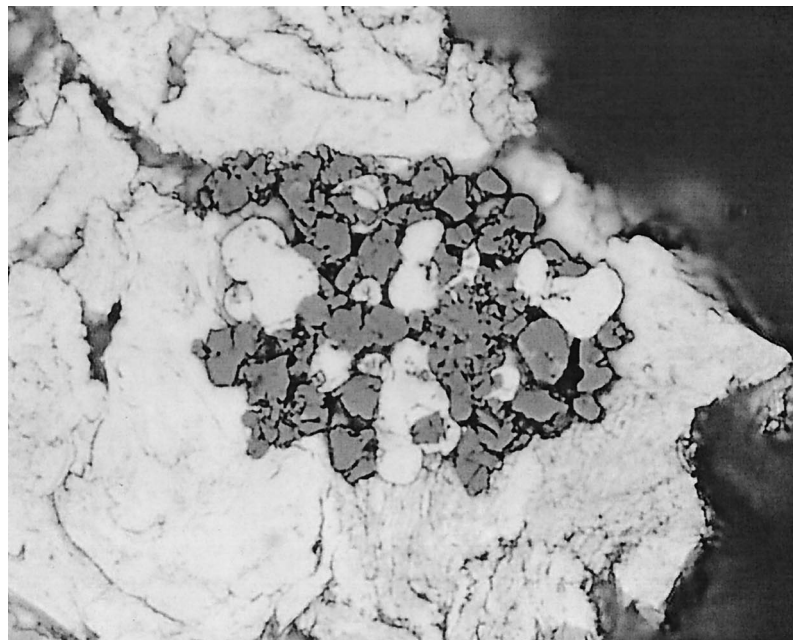


**Figure 12.** Measurement of eutectic temperatures of a mixture of Fe and FeO. Top panel shows before heating. Dark FeO grains are embedded in a Fe foil. Bottom panel shows after heating just above the eutectic temperature. Eutectic melting and subsequent recrystallization resulted in textural changes clearly visible under the microscope. Size of dark area is about 40  $\mu\text{m}$ .

cell. Fine powder of FeO was pressed into a disc of iron and then heated at 12 GPa to 1900 K, which is below the melting temperatures of both FeO and Fe and just above the solidus temperature, which is known at low pressure [Ringwood and Hibberson, 1990]. The shape of the sample was essentially unaltered due to the use of an argon pressure medium and by avoiding large temperature gradients. Textural changes are clearly evident on the recovered sample (see Figure 12).

The data for the Fe-FeS system to over 60 GPa [Boehler, 1996a] using the laser interference method deviate significantly from previous predictions of large melting depressions at higher pressures [Usselman, 1975] in that the melt depression decreases with pressure (see Figure 13). The estimated melting temperature of FeS at core pressures, which is obtained from diamond cell and shock measurements [Anderson and Ahrens, 1996; Boehler, 1992], is a few hundred degrees

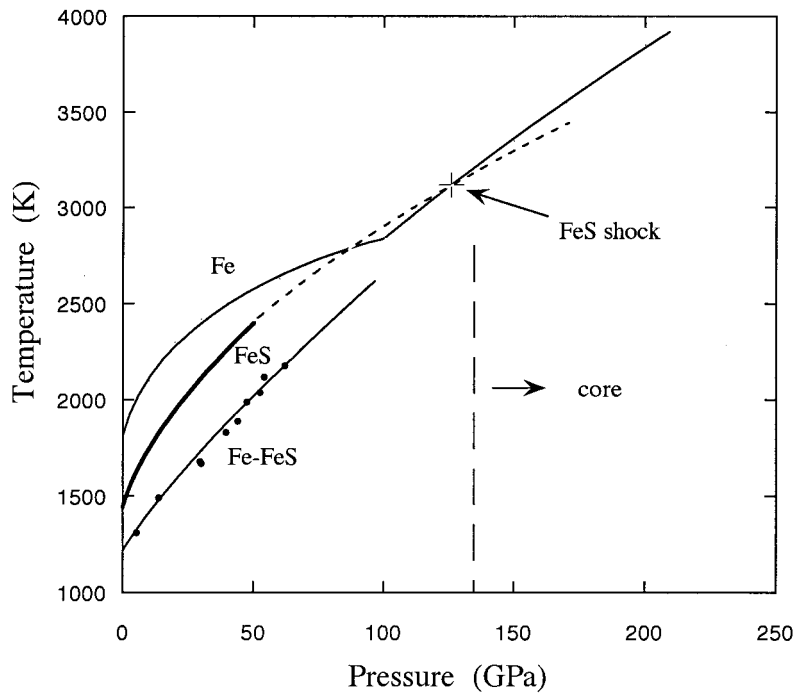


**Figure 13.** Melting temperatures of iron [Boehler, 1993], FeS [Boehler, 1992], and eutectic temperatures [Boehler, 1996a]. The static melting curve of FeS extrapolates to the shock melting point [Anderson and Ahrens, 1996]. The melting depression of iron due to the addition of sulfur decreases with pressure.

below the iron melting temperature. Thus a small melt depression of iron has to be expected. This lowers the estimated temperature at the inner core boundary to below 5000 K. The temperature on the core side of the core-mantle boundary (CMB) calculated from an outer core adiabat is then below 4000 K. Consequences of estimates of CMB temperatures significantly below 4000 K will be discussed below.

## 5. MELTING TEMPERATURES OF $(\text{Mg}, \text{Fe})\text{SiO}_3$ -PEROVSKITE AND $(\text{Mg}, \text{Fe})\text{O}$ -MAGNESIOWÜSTITE AND THE SOLIDUS OF THE LOWER MANTLE

Although the lower mantle is solid, its melting properties are key to understanding its chemical differentiation, which required a partially molten state. If the early Earth was hotter by a few hundred degrees than today, large parts of the upper mantle and transition zone were above the solidus, which is known for peridotite compositions. The depth range of partial melting of the lower mantle, however, is constrained by a melting behavior that is significantly different from that of the upper mantle and transition zone, owing to the entirely different structures of the materials. Experimental data have only become available very recently and will be reported here.

Two further issues are closely related to the melting behavior of lower mantle materials. One is the depth dependence of the viscosity, which is key to convection models. At low pressures it was found that the viscosity of a material directly scales with the homologous tem-

perature, which is the ratio of the temperature  $T$  to the melting temperature  $T_m$  [Weertman and Weertman, 1975]. The other issue comes from seismic observation from the core-mantle boundary, indicating a drastic drop in the sound velocities in a zone just above the core [e.g., Wen and Helmberger, 1998]. The question is whether this is due to a change in chemical composition or to melting. The magnitude in the velocity change, especially in the shear velocity, favors melting. If this is the case, there will be a further constraint on the temperature at the core-mantle boundary from the solidus temperature of the mantle.

Even though the exact chemical composition of the lower mantle is not known, one may assume that there are three major components:  $(\text{Mg}, \text{Fe})\text{SiO}_3$ -perovskite and  $(\text{Mg}, \text{Fe})\text{O}$ -magnesiowüstite, making up about 90%, and  $\text{CaSiO}_3$ -perovskite [Kesson et al., 1998]. On the basis of the phase diagram measured in multianvil presses to about 25 GPa and the very high melting temperature of  $\text{MgO}$  at ambient pressure, it was assumed that the eutectic composition of the lower mantle lies near the composition of the major component  $(\text{Mg}, \text{Fe})\text{SiO}_3$ -perovskite and that therefore, the melting temperature of perovskite would be near the lower mantle solidus. This is schematically shown in the phase diagram in Figure 14, suggested by Ito and Katsura [1992].

The large number of theoretical and experimental estimates of the melting temperature of  $(\text{Mg}, \text{Fe})\text{SiO}_3$ -perovskite for lower mantle pressures showed extremely large variation and will not be reviewed here (this is done elsewhere, for example, by Shen and Heinz [1998]).

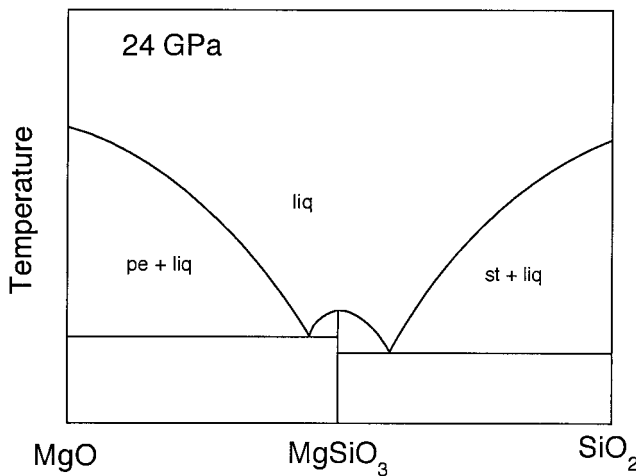


**Figure 14.** Schematic phase diagram of the MgO-SiO<sub>2</sub> system based on multianvil work [Ito and Takahashi, 1987]. At about 24 GPa the composition and melting temperature of MgSiO<sub>3</sub>-perovskite are near the eutectic.

Theoretical estimates are complicated due to the complex interatomic bonds and the poorly known thermodynamic properties, and the early melting experiments in the laser-heated diamond cells used unsuitable lasers and inadequate techniques for temperature measurement (see above).

New laser-heating techniques for the direct heating of minerals were developed with three major new features, all of which are key to producing uniform temperatures: (1) the use of CO<sub>2</sub> lasers with about 10 times higher power and a wavelength of about 10 μm, at which

minerals fully absorb the laser radiation, (2) the use of very thin samples, of the order of 10 μm, to reduce axial temperature gradients, and (3) the use of a hydrostatic pressure medium with low thermal conductivity, which reduces not only the pressure gradients but also the temperature gradients caused by the highly conductive diamond anvils. Melting was measured *in situ* by the large change in the optical absorption at the melt transition. First measurements on (Mg,Fe)SiO<sub>3</sub>-perovskite revealed a drastic increase in the melting temperatures with increasing pressures [Zerr and Boehler, 1993; Shen and Lazor, 1995]. Similar high melting slopes were measured for Ca-perovskite [Shen and Lazor, 1995; Zerr et al., 1997]. In contrast, the melting curve of MgO measured with the same method resulted in a rather shallow melting curve [Zerr and Boehler, 1994] that crosses that of perovskite between 40 and 50 GPa. These results are shown in Figure 15. The data for iron-free perovskite and that containing 10% Fe are combined for simplification.

The difference in the melting slopes between perovskite and MgO will significantly change the previously suggested phase diagram shown in Figure 14 at higher pressures. If phase rules observed at low pressure [Bridgeman, 1952; Ito and Katsura, 1992] are applied, the eutectic melting composition has to move away from that of (Mg,Fe)SiO<sub>3</sub>-perovskite and has to become (Mg, Fe)O-rich. This is illustrated schematically in Figure 16. With respect to the major elements, the composition of the lower mantle most likely lies somewhere between MgO and MgSiO<sub>3</sub>-perovskite. The addition of small amounts of iron has little effect on the melting temperature of perovskite [Zerr and Boehler, 1993] but lowers

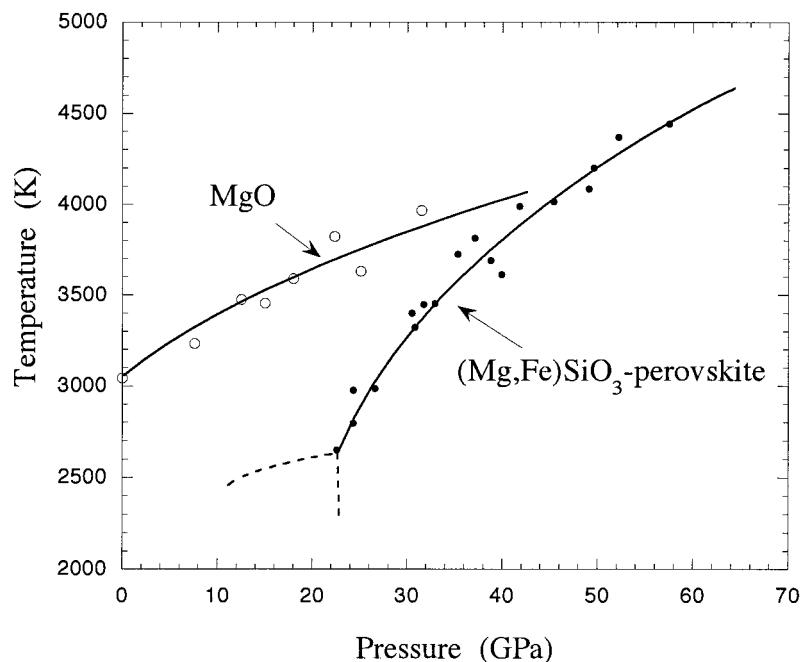


**Figure 15.** Melting curves of the two major lower mantle components MgO and (Mg,Fe)SiO<sub>3</sub>-perovskite measured in the diamond cell [Zerr and Boehler, 1993; Zerr and Boehler, 1994]. The addition of iron slightly lowers the melting temperatures of MgO.

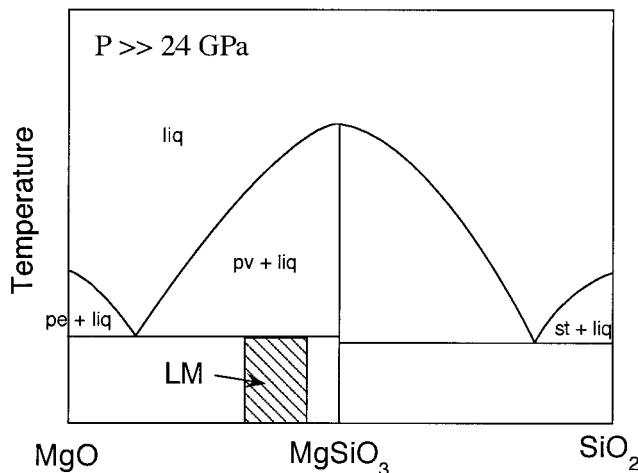


**Figure 16.** Schematic phase diagram of the  $\text{MgO}-\text{SiO}_2$  system at lower mantle pressures based on the melting temperatures shown in Figure 14. Melting temperatures of  $\text{MgSiO}_3$ -perovskite are higher than those of the end-members  $\text{MgO}$  and  $\text{SiO}_2$ . This shifts the eutectic composition toward  $\text{MgO}$  (or  $\text{SiO}_2$ ). The approximate lower mantle composition with respect to the major elements lies on the perovskite-rich side. At the solidus the lower mantle melt will be  $\text{MgO}$ -rich.

the melting temperature of  $\text{MgO}$  to somewhere between the melting curves of  $\text{MgO}$  and  $\text{FeO}$ , which are nearly parallel. There is experimental evidence that Fe partitions favorably into  $(\text{Mg}, \text{Fe})\text{O}$ -magnesiowüstite [Kesson and Fitz Gerald, 1992], and thus at very high pressure the first melt in a lower mantle system should be rich in  $(\text{Mg}, \text{Fe})\text{O}$ -magnesiowüstite.

Because the solidus is unlikely to be close to the melting temperature of a lower mantle end-member mineral, we investigated materials composed of all the major elements in the lower mantle: O, Si, Mg, Fe, Al, Ca, Ti, Cr, Ni, and Na (a *pyrolite* composition). As was described above, the amount of melt in a eutectic system may be very small as the solidus temperature is crossed, and a straightforward *in situ* optical detection of the onset of melting is extremely difficult. Therefore yet a new method to detect melting was developed and checked against previous measurements. Below about 25 GPa the solidus of peridotite, which has a close to pyrolytic composition, has been thoroughly investigated in multianvil presses [Ito and Takahashi, 1987; Takahashi, 1986; Zhang and Herzberg, 1994], and the new results are in good agreement with this previous work. The solidus temperatures were bracketed on the basis of textural changes observed in the recovered samples from a series of  $P$ - $T$  runs. For the diamond cell measurements, where the sample dimensions are of the order of 30  $\mu\text{m}$ , chemically homogeneous starting materials in the form of glass with pyrolytic composition had to be synthesized. A thin ( $\sim 10 \mu\text{m}$ ) sliver of this glass was heated to a given temperature with a  $\text{CO}_2$  laser in an argon pressure medium, and the recovered sample was subsequently examined by electron microscopy and

atomic force microscopy. These microscopic techniques allow the detection of submicroscopic changes in the recovered samples. Above the solidus temperature, distinctive recrystallization features associated with melting could be observed in addition to the subsolidus crystallization to the high-pressure phases, which were identified by Raman spectroscopy (see Figure 17). The temperatures at which these features occurred were identical to the previously reported solidus temperatures. Because this method is rather time-consuming, only a limited amount of solidus temperatures were measured up to about 60 GPa (see Figure 18). The measured pyrolyte solidus for this multicomponent system [Zerr *et al.*, 1998] lies approximately parallel to the melting curve of magnesiowüstite but is offset to lower temperatures by about 700 K. The melting curve of  $\text{MgO}$  (or magnesiowüstite) follows a Lindemann equation and yields very good agreement with the one atmosphere value of the Grüneisen parameter. Recently, a shock melting point of  $4300 \pm 270$  K at 130 GPa [Holland and Ahrens, 1997] of  $(\text{Mg}, \text{Fe})_2\text{SiO}_4$ -olivine was measured. Olivine is expected to break down to a perovskite-magnesiowüstite assemblage. The pyrolyte solidus, extrapolated along the same path as  $\text{MgO}$ , coincides with the shock melting point of olivine. Therefore a reasonable estimate for the solidus temperatures at the CMB (135 GPa) is about 4300 K.

### 5.1. Implications for Rheological Properties and Partial Melting in the Lower Mantle

On the basis of the assumption that the eutectic composition in the deep lower mantle is near that of  $(\text{Mg}, \text{Fe})\text{SiO}_3$ -perovskite, as implied from measurements at lower pressures (see above), a strong increase in the viscosity with depth was estimated [van Keken and Yuen, 1995; van Keken *et al.*, 1994] based on the steep melting slope of that material [Zerr and Boehler, 1993]. In these estimates it was assumed that the viscosity scales with the homologous temperature,  $T/T_m$ , the ratio of temperature to melting temperature [Weertman and Weertman, 1975], as is observed at low pressures. There are, of course, large uncertainties in these estimates, coming from the unknown actual temperature profile in the lower mantle, the complexity in a multicomponent system, and the mineral composition. Thermal conduction from the core, and radioactive heating in the mantle, are likely to change the temperature profile significantly from an *adiabatic temperature gradient*, and therefore the homologous temperature may not be a smooth function with depth. Moreover, rheological properties of a multicomponent system are difficult to estimate when the viscosities of the various components are significantly different from one another, as is the case for the major lower mantle phases (perovskites and magnesiowüstite). However, applying a Weertman model to the lower mantle, the viscosity change may be evaluated qualitatively: The average adiabatic temperature rise in the lower mantle has been estimated by various methods

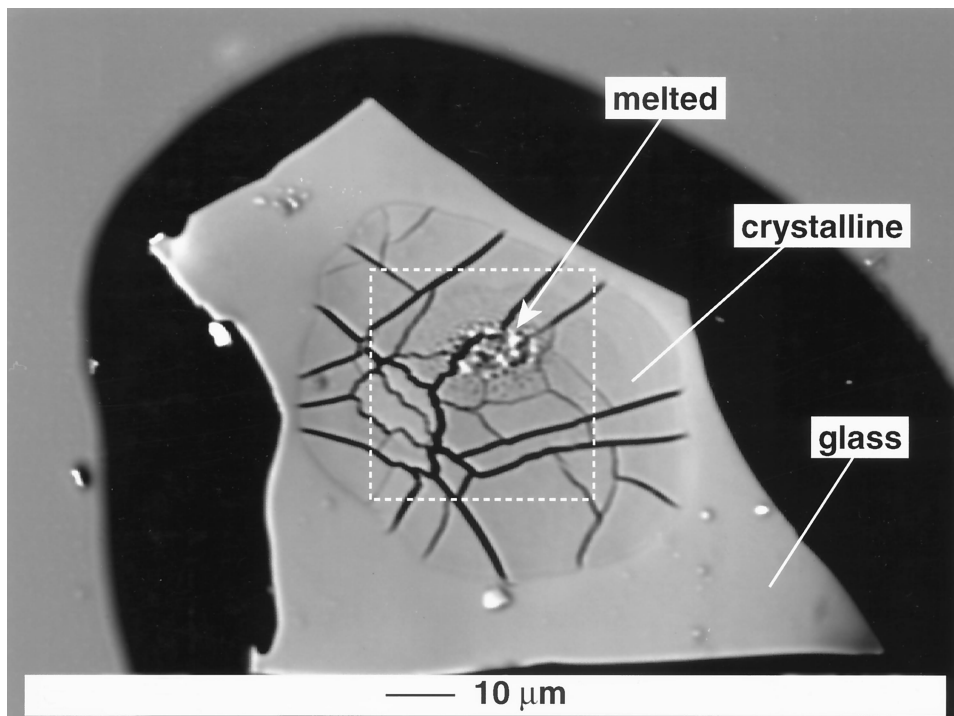


**Figure 17.** Glass sample with a pyrolytic composition heated with a  $\text{CO}_2$  laser in an argon pressure medium to 2550 K at 21 GPa (backscattering electron topographic image) [Zerr *et al.*, 1998]. Owing to the temperature gradient, the outer portion of the sample remains glass. At higher temperatures, toward the center of the heated area, this glass transforms to the high-pressure polymorphs, and at the highest temperatures the sample partially melts, as is evident from a different type of recrystallization.

[Boehler, 1982; Brown and Shankland, 1981; Jeanloz and Richter, 1979; Stacey, 1977] and lies between  $0.25^\circ$  and  $0.3^\circ \text{ km}^{-1}$ . Even if strong curvature is applied for the extrapolation of the melting curve of  $(\text{Mg},\text{Fe})\text{SiO}_3$ -perovskite, the major component of the lower mantle, the average melting slope is still at least 3 times higher (see Figure 18). If the pyrolite solidus temperatures are extrapolated to the shock melting point of olivine, the average slope of the lower mantle solidus is between  $0.5^\circ$  and  $0.6^\circ \text{ km}^{-1}$ , or still about twice the average adiabatic gradient. Thus, because both melting temperatures of end-member components and eutectic temperatures relevant to the lower mantle change more rapidly than the average mantle temperature (decrease of the homologous temperature), an increase in the average viscosity in the lower mantle may be expected.

## 5.2. Partial Melting in the Lower Mantle

Our solidus temperatures are between 900 and 1600 K above the average lower mantle adiabat (see Figure 18). This fact excludes large-scale melting of the lower mantle, except for the case of large impacts. If the Earth cooled in a steady state manner, only a thin layer at the bottom of the lower mantle could have been partially molten. In the absence of a *thermal boundary layer* between upper and lower mantle, the temperature at the top of the lower mantle, at a depth of 660 km, is  $1900 \pm 100$  K, obtained from laboratory measurements of the

phase boundary of  $(\text{Mg},\text{Fe})\text{SiO}_3$ -perovskite (see above). At that depth the solidus temperature is 2800 K. At the CMB the extrapolated solidus temperature is about 4300 K. This is near the temperature of the outer core at the CMB, as deduced from melting temperature measurements on the Fe-O-S system ( $4000 \pm 200$  K) [Boehler, 1996b]. Thus it is possible to have partial melting of the mantle at the core-mantle boundary.

Seismic measurements reveal a drastic decrease in the seismic velocities in a thin zone at the CMB (*ultra low velocity zone*) [e.g., Garnero *et al.*, 1993; Revenough and Meyer, 1997; Wen and Helmberger, 1998], especially in the region of hot spots [Helmberger *et al.*, 1998; Russel *et al.*, 1998]. The magnitude of this velocity change is difficult to explain other than being due to partial melting. This is a plausible explanation because the temperature at the very bottom of the mantle in direct contact with the core reaches the core temperature of  $4000 \pm 200$  K, which is close to the mantle solidus. Changes in the chemical and/or mineral composition, listed below, may also occur at the CMB, but these are unlikely to cause the large drop in the sound velocities that are observed.

1. It has been suggested that the core-mantle boundary may be a zone of intensive chemical reaction and that the lower mantle material may become enriched in iron [Knittle and Jeanloz, 1991]. More recent measurements on the chemical interaction between molten iron

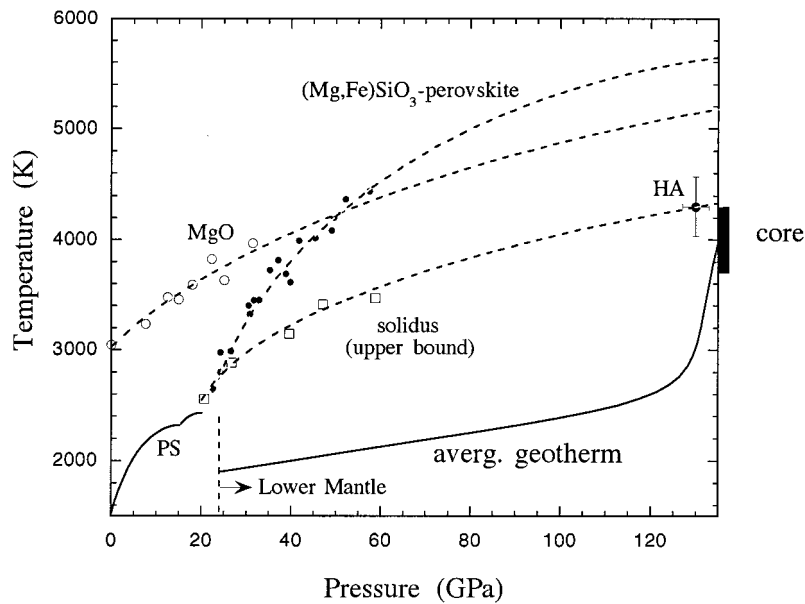


**Figure 18.** Melting condition in the lower mantle. The measured solidus temperatures [Zerr *et al.*, 1998] are upper bounds. An extrapolation parallel to the MgO melting curve yields agreement with the olivine shock melting point [Holland and Ahrens, 1997]. At the core-mantle boundary (CMB) the solidus temperature is near the core temperature derived from the melting of iron. The average geotherm follows an adiabat, with a large temperature jump at the CMB. This allows partial melting in a thin zone above the core. “PS” is an average of peridotite solidus temperatures measured in multianvil presses.

and lower mantle materials, however, showed that these chemical interactions are limited to subpercent levels [Hillgren and Boehler, 1998, 2000] and are thus unlikely to cause significant velocity changes.

2. At the pressure of the core mantle boundary,  $(\text{Mg}_{0.88}\text{Fe}_{0.12})\text{O}$ -magnesiowüstite is about 2% more dense than  $(\text{Mg}_{0.88}\text{Fe}_{0.12})\text{SiO}_3$ -perovskite [Chopelas and Boehler, 1992]. If liquid  $(\text{Mg},\text{Fe})\text{O}$ -magnesiowüstite (most likely enriched in iron) would segregate in a partially molten mantle by gravity, the velocities would be likely to increase in a magnesiowüstite-enriched layer.

3. The same is true if  $(\text{Mg},\text{Fe})\text{SiO}_3$ -perovskite would break down to its oxides  $\text{SiO}_2$  and  $(\text{Mg},\text{Fe})\text{O}$ -magnesiowüstite, as has been recently suggested [Saxena *et al.*, 1996b]. This assemblage would have to be denser than  $(\text{Mg},\text{Fe})\text{SiO}_3$ -perovskite. Moreover, it has been shown that such a breakdown is highly unlikely [Sergiou *et al.*, 1998].

4. There is a possibility that the core-mantle boundary is a zone of accumulated subducted slab material, but the density difference between such material and the surrounding mantle is very small [Kesson *et al.*, 1998]. Therefore, at present, the extrapolated solidus temperature, the shock melting temperature of olivine, and the estimated core temperature from the melting temperature of the iron-oxygen-sulfur system are in accordance with a melting interpretation of the seismic evidence. For core temperatures, which are significantly lower than those derived above, partial melting in the lower mantle is not a solution for the seismic observation.

## 6. FUTURE EXPERIMENTS

It may be difficult to significantly expand the pressure range and accuracy of melting experiments in the diamond cell. Higher laser power and the design of even higher-resolution collecting optics may provide some improvement with regard to temperature gradients and visual observation of phase transitions.

A large effort should be made to understand the chemical reactions that occur under extreme pressure and temperature conditions. Samples from diamond cell experiments can be quantitatively analyzed using special sample preparation in combination with electron microprobes and ion probes (*secondary ion mass spectrometry (SIMS)*) [Hillgren and Boehler, 1998, 2000; Tschauner *et al.*, 1999]. These are the first quantitative measurements of the chemical interaction between core and mantle materials. The chemical analysis of minute partial melt fractions to study solid-liquid element partitioning at very high pressures requires the further development of submicron analytical methods (for example, nano-SIMS).

The submicron chemical analysis of diamond cell samples will also help to better understand chemical reactions of samples with different pressure media (including noble gases) and the effect of light elements on the melting temperature of iron. In most iron melting experiments,  $\text{Al}_2\text{O}_3$  or other oxides were used as pressure media. Chemical reactions, not obvious in these experiments, cannot be excluded, especially when a layer

only a few nanometers thick is involved in the melting process at very high pressure. Although melting temperatures measured in an argon pressure medium agree with those measured in  $\text{Al}_2\text{O}_3$  to pressures of 35 GPa [Boehler *et al.*, 1990], iron samples recovered from pressures in the 100-GPa range have to be routinely analyzed.

Shock sound velocity measurements should be continued in order to solve the present uncertainty in the onset of melting of iron. Further shock experiments on preheated iron would be very useful to check the melting temperature and the phase diagram at lower pressures. X-ray measurements on laser-heated iron using modern synchrotron techniques must be performed in an inert, hydrostatic pressure medium and by minimizing temperature gradients in order to solve the present disagreement of results.

## GLOSSARY

**Adiabatic temperature gradient:** Temperature variation with depth due only to the compression of the material. In a convecting system like the Earth's mantle, assuming constant viscosity and without internal heating, the temperature-depth profile lies along an adiabat [McKenzie *et al.*, 1974] (see Grüneisen parameter).

**Charge-coupled device (CCD) detector:** A two-dimensional array of silicon diodes.

**Chromatic aberration:** Difference in focal length of a lens at different wavelengths (see Figure 3).

**dhcp:** Double hexagonally close-packed, similar to hcp with different stacking order.

**Dichroic mirrors:** Mirrors that reflect only in a specific wavelength range, for example, are transmissible for laser radiation at 1  $\mu\text{m}$  wavelength but reflect visible light.

**Emissivity:** Ratio of the emissive powers of a real (gray) body and an ideal (black) body.

**Grüneisen parameter:** Frequently used in geophysics, shock physics, and theoretical high-temperature equations of state. Parameter is related to the adiabatic gradient by  $\gamma = K_S/T(dT/dP)_S = \alpha K_T/c_P \rho = \alpha K_T/c_V \rho$ , where  $K_S$  and  $K_T$  are the adiabatic and isothermal bulk moduli  $K_{S,T} = -V(dP/dV)_{S,T}$ ;  $\alpha$  is the thermal expansion coefficient  $\alpha = 1/V(dV/dT)_V$ ;  $c_p$  and  $c_V$  are the specific heats at constant pressure and volume, respectively; and  $\rho$  is the density.

**hcp:** Hexagonally close-packed.

**Hugoniot:** Pressure-volume-temperature relationship during shock compression, material specific (usually pressure-volume plot).

**Lindemann melting relation:** Not a melting theory but relates melting to the amplitude of atomic vibration (see Poirier [1991] for a review).

**Molecular dynamics simulation:** Computer simulations of a large number of interacting particles; yields structural, thermodynamic, and transport properties.

**Powder diffraction:** X-ray diffraction method using polycrystalline samples; yields lattice constants.

**Pyrolite:** Fictitious model rock with a chemical composition of mainly olivine and orthopyroxene, some calcic clinopyroxene, and an aluminous phase (e.g., garnet).

**Raman spectroscopy:** Scattering of monochromatic laser light, which produces a spectrum based on the change in polarizability during atomic vibrations. This yields information about the vibrational frequencies in a solid.

**Seismic anisotropy:** Directional variation of seismic velocity.

**Secondary ion mass spectrometry (SIMS):** Chemical analytical method with high spatial resolution.

**Solidus temperature:** Temperature at which the first melt is produced in a multicomponent system.

**Synchrotron radiation:** Electromagnetic radiation emitted by electrons or positrons orbiting in a storage ring. This radiation results from the centripetal acceleration of the electrons by the magnetic fields in the ring. The spectrum contains high-energy X rays with high intensity, useful for X-ray diffraction on very small samples.

**Yield strength:** Stress above which a material deforms plastically (elastic limit).

**Thermal boundary layer:** Layer in which the thermal gradient deviates from an adiabat due to thermal conduction. Heat transfer through the boundary layer controls the cooling of the Earth.

**Thermal expansion coefficient:**  $\alpha = 1/V(dV/dT)_P$ . In the Earth, values range from 1 to  $5 \times 10^{-5} \text{ K}^{-1}$ .

**Thermal pressure:** Pressure increase due to heating at constant volume:  $P_{TH} = \alpha K_T \Delta T$ .

**Ultra-low-velocity zone:** A thin (5–40 km thick) layer above the core-mantle boundary (at a depth of 2900 km), where a reduction of the seismic velocities of 10% and more has been observed.

**ACKNOWLEDGMENTS.** I thank Anne Hofmeister for her constructive review. The paper was improved by a critical reading by Valerie Hillgren.

Tilman Spohn was the Editor responsible for this paper. He thanks Anne Hofmeister and Tom Ahrens for technical reviews and an anonymous cross-disciplinary reviewer.

## REFERENCES

- Ahrens, T. J., G. Q. Chen, and K. G. Holland, Phase diagram of iron, revised-core temperatures, *Geophys. Res. Lett.*, in press, 2000.
- Anderson, O. L., Properties of iron at the Earth's core conditions, *Geophys. J. R. Astron. Soc.*, 84, 561–579, 1986.
- Anderson, O. L., The phase diagram of iron and the temperature of the inner core, *J. Geomagn. Geoelectr.*, 45, 1235–1248, 1993.
- Anderson, W. W., and T. J. Ahrens, An equation of state for liquid iron and implications for the Earth's core, *J. Geophys. Res.*, 99, 4273–4284, 1994.

- Anderson, W. W., and T. Ahrens, Shock temperature and melting in iron sulfides at core pressures, *J. Geophys. Res.*, **101**, 5627–5642, 1996.
- Anderson, O. L., and A. Duba, Experimental melting curve of iron revisited, *J. Geophys. Res.*, **102**, 22,659–22,669, 1997.
- Andrault, D., G. Fiquet, M. Kunz, F. Visocekas, and D. Häusermann, The orthorhombic structure of iron: An in situ study at high temperature and high pressure, *Science*, **278**, 831–834, 1997.
- Belonoshko, A. B., Atomistic simulation of shock wave-induced melting in argon, *Science*, **275**, 955–957, 1997.
- Boehler, R., Measurement of the adiabats of quartz, forsterite, and magnesium oxide at high pressures and high temperatures and adiabatic gradients in the mantle of the Earth, *Phys. Earth Planet. Inter.*, **29**, 105–107, 1982.
- Boehler, R., The phase diagram of iron to 430 kbar, *Geophys. Res. Lett.*, **13**, 1153–1156, 1986.
- Boehler, R., Melting of the Fe-FeO and the Fe-FeS systems at high pressure: Constraints on core temperatures, *Earth Planet. Sci. Lett.*, **111**, 217–227, 1992.
- Boehler, R., Temperatures in the Earth's core from melting-point measurements of iron at high static pressures, *Nature*, **363**, 534–536, 1993.
- Boehler, R., Fe-FeS eutectic temperatures to 620 kbar, *Phys. Earth Planet. Inter.*, **96**, 181–186, 1996a.
- Boehler, R., Melting temperature of the Earth's mantle and core: Earth's thermal structure, *Annu. Rev. Earth Planet. Sci.*, **24**, 15–40, 1996b.
- Boehler, R., and A. Chopelas, A new approach to laser heating in high-pressure mineral physics, *Geophys. Res. Lett.*, **18**, 1147–1150, 1991.
- Boehler, R., and A. Chopelas, Phase transitions in a 500 kbar–3000 K gas apparatus, in *High-Pressure Research: Application to Earth and Planetary Sciences*, edited by Y. Syono and M. H. Manghnani, pp. 55–60, Terra Sci., Tokyo, 1992.
- Boehler, R., and J. Ramakrishnan, Experimental results on the pressure dependence of the Grüneisen parameter: A review, *J. Geophys. Res.*, **85**, 6996–7002, 1980.
- Boehler, R., and M. Ross, Melting curve of aluminum in a diamond cell to 0.8 Mbar: Implications for iron, *Earth Planet. Sci. Lett.*, **153**, 223–227, 1997.
- Boehler, R., and D. A. Young, Melting and adiabats of the alkali metals at high compressions, *J. Non Cryst. Solids*, **61**, 141–146, 1984.
- Boehler, R., N. von Bargen, and A. Chopelas, Melting, thermal expansion, and phase transitions of iron at high pressures, *J. Geophys. Res.*, **95**, 21,731–21,736, 1990.
- Boehler, R., M. Ross, and D. B. Boercker, High pressure melting curves of alkali halides, *Phys. Rev. B*, **53**, 556–563, 1996.
- Boehler, R., M. Ross, and D. B. Boercker, Melting of LiF and NaCl to 1 Mbar: Systematics of ionic solids at extreme conditions, *Phys. Rev. Lett.*, **78**, 4589–4592, 1997.
- Boness, D. A., and J. M. Brown, The electronic band structures of iron, sulfur, and oxygen at high pressures and the Earth's core, *J. Geophys. Res.*, **95**, 21,721–21,730, 1990.
- Boness, D. A., and J. M. Brown, Bulk superheating of solid KBr and CsBr with shock waves, *Phys. Rev. Lett.*, **71**, 2931–2934, 1993.
- Bridgman, P. W., *The Physics of High Pressure*, p. 220, G. Bell, London, 1952.
- Brown, J. M., and R. G. McQueen, Phase transitions, Grüneisen parameter, and elasticity for shocked iron between 77 GPa and 400 GPa, *J. Geophys. Res.*, **91**, 7485–7494, 1986.
- Brown, J. M., and T. S. Shankland, Thermodynamic parameters in the Earth as determined from seismic profiles, *Geophys. J. R. Astron. Soc.*, **66**, 579–596, 1981.
- Chopelas, A., Estimates of mantle relevant Clapeyron slopes in the MgSiO<sub>3</sub> system from high pressure spectroscopic data, *Am. Mineral.*, **84**, 233–244, 1999.
- Chopelas, A., and R. Boehler, Thermal expansivity in the lower mantle, *Geophys. Res. Lett.*, **19**, 1983–1986, 1992.
- Dreibus, G., and H. Palme, Cosmochemical constraints on the sulfur content in the Earth's core, *Geochim. Cosmochim. Acta*, **60**, 1125–1130, 1996.
- Dubrovinsky, L. S., S. K. Saxena, and P. Lazor, High-pressure and high temperature in situ X-ray diffraction study of iron and corundum to 68 GPa using an internally heated diamond anvil cell, *Phys. Chem. Miner.*, **25**, 434–441, 1998.
- Dziewonski, A. M., and D. L. Anderson, Preliminary reference Earth model, *Phys. Earth Planet. Inter.*, **25**, 297–356, 1981.
- Fiquet, G., D. Andrault, J. P. Itié, P. Gillet, and P. Richet, X-ray diffraction of periclase in a laser-heated diamond-anvil cell, *Phys. Earth Planet. Inter.*, **95**, 1–17, 1996.
- Gallagher, K. G., J. D. Bass, T. J. Ahrens, M. Fitzner, and J. R. Abelson, Shock temperature of stainless steel and a high pressure–high temperature constraint on thermal diffusivity of Al<sub>2</sub>O<sub>3</sub>, in *High-Pressure Science and Technology*, edited by S. C. Schmidt et al., pp. 963–966, Am. Inst. Phys., College Park, Md., 1993.
- Garnero, E. J., S. P. Grand, and D. V. Helmberger, Low *p*-wave velocity at the base of the mantle, *Geophys. Res. Lett.*, **20**, 1843–1846, 1993.
- Getting, I. C., and G. C. Kennedy, Effect of pressure on the emf of chromel-alumel and platinum-platinum 10% rhodium thermocouples, *J. Appl. Phys.*, **41**, 4552–4562, 1970.
- Heinz, D. L., and R. Jeanloz, Temperature measurements in the laser-heated diamond cell, in *High-Pressure Research in Mineral Physics*, *Geophys. Monogr. Ser.*, vol. 39, edited by M. H. Manghnani and Y. Syono, pp. 113–128, AGU, Washington, D. C., 1987.
- Helmberger, D. V., L. Wen, and X. Ding, Seismic evidence that the source of the Iceland hotspot lies at the core–mantle boundary, *Nature*, **396**, 251–255, 1998.
- Hillgren, V. J., and R. Boehler, High pressure reactions between metals and silicates: Implications for the light element in the core and core–mantle interactions (abstract), *Mineral. Mag.*, **62A**, 624–625, 1998.
- Hillgren, V. J., and R. Boehler, High pressure geochemistry in the diamond cell to 100 GPa and 330 K, *High Pressure Sci. Technol.*, *Proc. AIRAPT Int. Conf.*, in press, 2000.
- Holland, K. G., and T. J. Ahrens, Melting of (Mg,Fe)<sub>2</sub>SiO<sub>4</sub> at the core–mantle boundary of the Earth, *Science*, **275**, 1623–1625, 1997.
- Irifune, T. E. A., The postspinel phase boundary in Mg<sub>2</sub>SiO<sub>4</sub> determined by in situ X-ray diffraction, *Science*, **279**, 1698–1700, 1998.
- Ito, E., and T. Katsura, Melting of ferromagnesian silicates under the lower mantle conditions, in *High-Pressure Research: Application to Earth and Planetary Sciences*, edited by Y. Syono and M. H. Manghnani, pp. 315–322, Terra Sci., Tokyo, 1992.
- Ito, E., and E. Takahashi, Melting of peridotite at uppermost lower-mantle conditions, *Nature*, **328**, 514–517, 1987.
- Ito, E., and E. Takahashi, Postspinel transformations in the system Mg<sub>2</sub>SiO<sub>4</sub>–Fe<sub>2</sub>SiO<sub>4</sub> and some geophysical implications, *J. Geophys. Res.*, **94**, 10,637–10,646, 1989.
- Jeanloz, R., and F. M. Richter, Convection, composition, and the thermal state of the lower mantle, *J. Geophys. Res.*, **84**, 5497–5504, 1979.
- Jephcoat, A. P., and S. P. Besedin, Temperature measurement and melting determination in the laser-heated diamond-anvil cell, in *Philosophical Transactions: Development in High-Pressure, High-Temperature Research and the Study of the Earth's Deep Interior*, vol. 354, edited by A. P. Jephcoat, R. J. Angel, and R. K. O'Nions, pp. 1333–1360, R. Soc. of London, London, 1996.

- Katsura, T., and E. Ito, The system  $Mg_2SiO_4$ - $Fe_2SiO_4$  at high pressures and temperatures: Precise determination of stabilities of olivine, modified spinel, and spinel, *J. Geophys. Res.*, 94, 15,663–15,670, 1989.
- Kellogg, L. H., B. H. Hager, and R. D. van der Hilst, Compositional stratification in the deep mantle, *Science*, 283, 1881–1884, 1999.
- Kesson, S. E., and J. Fitz Gerald, Partitioning of  $MgO$ ,  $FeO$ ,  $NiO$ ,  $MnO$ , and  $Cr_2O_3$  between magnesium silicate perovskite and magnesiowüstite: Implications for the origin of inclusions in diamond and the composition of the lower mantle, *Earth Planet. Sci. Lett.*, 111, 229–240, 1992.
- Kesson, S. E., J. D. Fitz Gerald, and J. M. Shelly, Mineralogy and dynamics of a pyrolite lower mantle, *Nature*, 393, 253–255, 1998.
- Kingslake, R., *Lens Design Fundamentals*, p. 331, Harcourt Brace, Orlando, Fla., 1978.
- Knittle, E., and R. Jeanloz, Earth's core-mantle boundary: Results of experiments at high pressures and temperatures, *Science*, 251, 1438–1443, 1991.
- Kraut, E. A., and G. C. Kennedy, New melting law at high pressures, *Phys. Rev. Lett.*, 16, 608–609, 1966.
- Lyzenga, G. A., T. J. Ahrens, and A. C. Mitchell, Shock temperatures of  $SiO_2$  and their geophysical implications, *J. Geophys. Res.*, 88, 2431–2444, 1983.
- Mao, H. K., P. M. Bell, J. W. Shaner, and D. J. Steinberg, Specific volume measurements of Cu, Mo, Pd, and Ag and calibration of the ruby  $R_1$  fluorescence pressure gauge from 0.06 to 1 Mbar, *J. Appl. Phys.*, 49, 3276–3283, 1978.
- Mao, H. K., Y. Wu, L. C. Chen, J. F. Shu, and A. P. Jephcoat, Static compression of iron to 300 GPa and  $Fe_{0.8}Ni_{0.2}$  alloy to 260 GPa: Implications for composition of the core, *J. Geophys. Res.*, 95, 21,737–21,742, 1990.
- Masters, T. G., and P. M. Shearer, Summary of seismological constraints on the structure of the Earth's core, *J. Geophys. Res.*, 95, 21,691–21,695, 1990.
- McKenzie, D. P., J. M. Roberts, and N. O. Wei, Convection in the Earth's mantle: Toward a numerical simulation, *J. Fluid Mech.*, 62, 465–538, 1974.
- Ming, L. C., and W. A. Bassett, Laser heating in the diamond anvil press up to 2000°C sustained and 3000°C pulsed at pressures up to 260 kilobars, *Rev. Sci. Instrum.*, 9, 1115–1118, 1974.
- Nguyen, J. H., and N. C. Holmes, Iron sound velocities in shock wave experiments up to 400 GPa (abstract), *Eos Trans. AGU*, 79(45), Fall Meet. Suppl., F846, 1998.
- O'Neill, H. S. C., D. Canil, and D. C. Rubie, Oxide-metal equilibria to 2500°C and 25 GPa: Implications for core formation and the light component in the Earth's core, *J. Geophys. Res.*, 103, 12,239–12,260, 1998.
- Poirier, J. P., *Introduction to the Physics of the Earth's Interior*, edited by A. Putnis and R. C. Liebermann, Cambridge Univ. Press, New York, 1991.
- Poirier, J. P., Light elements in the Earth's outer core: A critical review, *Phys. Earth Planet. Inter.*, 85, 310–337, 1994.
- Ramakrishnan, J., R. Boehler, G. H. Higgins, and G. C. Kennedy, Behavior of Grüneisen's parameter of some metals at high pressures, *J. Geophys. Res.*, 83, 3535–3538, 1978.
- Ramakrishnan, J., R. J. Hardy, and G. C. Kennedy, The Grüneisen parameter  $\gamma$  of KBr, RbCl and Bi through high pressure phase transitions, *J. Phys. Chem. Solids*, 40, 297–303, 1979.
- Revenough, J. S., and R. Meyer, Seismic evidence of partial melt within a possible ubiquitous low velocity layer at the base of the mantle, *Science*, 277, 670–673, 1997.
- Ringwood, A. E., and W. Hibberson, The system Fe-FeO revisited, *Phys. Chem. Miner.*, 17, 313–319, 1990.
- Russel, S. A., T. Lay, and E. J. Garnero, Seismic evidence for small-scale dynamics in the lowermost mantle at the root of the Hawaiian hotspot, *Nature*, 396, 255–258, 1998.
- Saxena, S. K., G. Shen, and P. Lazor, Experimental evidence for a new iron phase and implications for the Earth's core, *Science*, 260, 1312–1314, 1993.
- Saxena, S. K., G. Shen, and P. Lazor, Temperatures in Earth's core based on melting and phase transformation experiments on iron, *Science*, 264, 405–407, 1994.
- Saxena, S. K., L. S. Dubrovinsky, and P. Häggkvist, X-ray evidence for the new phase  $\beta$ -iron at high temperature and high pressure, *Geophys. Res. Lett.*, 23, 2441–2444, 1996a.
- Saxena, S. K., L. S. Dubrovinsky, P. Lazor, Y. Cerenius, P. Häggkvist, M. Hanfland, and J. Hu, Stability of perovskite ( $MgSiO_3$ ) in the Earth's mantle, *Science*, 274, 1357–1359, 1996b.
- Sergiou, G., A. Zerr, and R. Boehler,  $(Mg,Fe)SiO_3$ -perovskite stability under lower mantle conditions, *Science*, 280, 2093–2095, 1998.
- Shen, G., and D. L. Heinz, High-pressure melting of deep mantle and core materials, in *Ultra-High-Pressure Mineralogy: Physics and Chemistry of the Earth's Deep Interior*, vol. 37, edited by R. J. Hemley, pp. 369–396, Mineral. Soc. of Am., Washington, D. C., 1998.
- Shen, G., and P. Lazor, Measurement of melting temperatures of some minerals under lower mantle pressures, *J. Geophys. Res.*, 100, 17,699–17,713, 1995.
- Shen, G., H. K. Mao, R. J. Hemley, T. S. Duffy, and M. L. Rivers, Melting and crystal structure of iron at high pressures and temperatures, *Geophys. Res. Lett.*, 25, 373–376, 1998.
- Sherman, D. M., Stability of possible Fe-FeS and Fe-FeO alloy phases at high pressure, *Earth Planet. Sci. Lett.*, 132, 87–98, 1995.
- Sherman, D., The composition of the Earth's core: New constraints on S and Si versus temperature, *Earth Planet. Sci. Lett.*, 153, 149–155, 1997.
- Song, X., and D. V. Helmberger, Seismic evidence for an inner core transition zone, *Science*, 282, 924–927, 1998.
- Stacey, F. D., A thermal model of the Earth, *Phys. Earth Planet. Inter.*, 15, 341–348, 1977.
- Stevenson, D. J., Models of the Earth's core, *Science*, 214, 611–619, 1981.
- Takahashi, E., Melting of a dry peridotite KLB-1 up to 14 GPa: Implications on the origin of peridotitic upper mantle, *J. Geophys. Res.*, 91, 9367–9382, 1986.
- Tschauner, O., A. Zerr, S. Specht, A. Rocholl, R. Boehler, and H. Palme, Partitioning of nickel and cobalt between metal and silicate perovskite up to 80 GPa, *Nature*, 398, 604–607, 1999.
- Urakawa, S., M. Kato, and M. Kumazawa, Experimental study of the phase relation in the system Fe-Ni-O-S up to 15 GPa, in *High-Pressure Research in Mineral Physics*, edited by M. H. Manghnani and Y. Syono, pp. 95–111, Terra Sci., Tokyo, 1987.
- Usselman, T. M., Experimental approach to the state of the core, part I, The liquidus relations of the Fe-rich portion of the Fe-Ni-S system from 30 to 100 kb, *Am. J. Sci.*, 275, 278–290, 1975.
- van Keken, P. E., and D. A. Yuen, Dynamical influences of high viscosity in the lower mantle induced by the steep melting curve of perovskite: Effects of curvature and time dependence, *J. Geophys. Res.*, 100, 15,233–15,248, 1995.
- van Keken, P. E., D. A. Yuen, and A. P. van den Berg, Implications for mantle dynamics from the high melting temperatures of perovskite, *Science*, 264, 1437–1439, 1994.
- Weertman, J., and J. R. Weertman, High temperature creep of rock and mantle viscosity, *Annu. Rev. Geophys.*, 3, 293–315, 1975.
- Wen, L., and D. V. Helmberger, Ultra-low velocity zones near

- the core-mantle boundary from broadband PKP precursors, *Science*, 279, 1701–1703, 1998.
- Williams, Q., R. Jeanloz, J. Bass, B. Svendsen, and T. J. Ahrens, The melting curve of iron to 2.5 Mbar: A constraint on the temperature of the Earth's core, *Science*, 236, 181–182, 1987.
- Yoo, C. S., J. Akella, and C. Ruddle, Melting studies of iron and uranium by DAC Laser heating experiments (abstract), *Eos Trans. AGU*, 73(43), Fall Meet. Suppl., 64, 1992.
- Yoo, C. S., N. C. Holmes, M. Ross, D. J. Webb, and C. Pike, Shock temperatures and melting of iron at Earth core conditions, *Phys. Rev. Lett.*, 70, 3931–3934, 1993.
- Yoo, C. S., P. Söderlind, J. A. Moriarty, and A. J. Campbell, dhcp as a possible new  $\epsilon'$  phase of iron at high pressures and temperatures, *Phys. Lett. A*, 214, 65–70, 1996.
- Zerr, A., and R. Boehler, Melting of  $(\text{Mg}, \text{Fe})\text{SiO}_3$ -perovskite to 625 kbar: Indication of a high melting temperature in the lower mantle, *Science*, 262, 553–555, 1993.
- Zerr, A., and R. Boehler, Constraints on the melting temperature of the lower mantle from high pressure experiments on MgO and magnesiowüstite, *Nature*, 371, 506–508, 1994.
- Zerr, A., G. Serghiou, and R. Boehler, Melting of  $\text{CaSiO}_3$ -perovskite to 430 kbar and first *in situ* measurements of lower mantle eutectic temperatures, *Geophys. Res. Lett.*, 24, 909–912, 1997.
- Zerr, A., A. Diegeler, and R. Boehler, Solidus of the Earth's deep mantle, *Science*, 281, 243–245, 1998.
- Zha, C. S., R. Boehler, D. A. Young, and M. Ross, The argon melting curve to very high pressures, *J. Chem. Phys.*, 85, 1034–1036, 1986.
- Zha, C. S., H. K. Mao, and R. J. Hemley, A primary pressure scale to 55 GPa from new measurements of equation of state and elasticity for MgO, *High Pressure Sci. Technol., Proc. AIRAPT Int. Conf.*, in press, 2000.
- Zhang, J., and C. Herzberg, Melting experiments on anhydrous peridotite KLB-1 from 5.0 to 22.5 GPa, *J. Geophys. Res.*, 99, 17,729–17,742, 1994.

---

R. Boehler, Hochdruck-Mineralphysik, Max-Planck Institut für Chemie, Postfach 3060, 55020 Mainz, Germany.  
(boe@mpch-mainz.mpg.de)

